frontiers in Chemical Engineering

TYPE Original Research
PUBLISHED 27 August 2026
DOI 10.3389/fceng.2026.1887485

Check for updates

OPEN ACCESS

EDITED BY
Jia Wei Chew,
Chalmers University of Technology, Sweden

REVIEWED BY
Mrudula Pulimi,
Vellore Institute of Technology (VIT), India
Sharon Fatinathan,
University of Kuala Lumpur, Malaysia

*CORRESPONDENCE
Sankha Chakrabortty,
sankha.chakrabortty@kiitbiotech.ac.in
Suraj K. Tripathy,
suraj.tripathy@kiitbiotech.ac.in
Jayato Nayak,
nayak.jayato@gmail.com
Ramesh Kumar,
rameshibt@hanyang.ac.kr

RECEIVED 21 May 2026
REVISED 21 July 2026
ACCEPTED 31 July 2026
PUBLISHED 27 August 2026

CITATION
Mishra S, Khare D, Kumar R, Banerjee S, Jeon B-H, Nayak J, Chakrabortty S and Tripathy SK (2026) Mechanistic insight into CBB-G removal by NiO@chitosan beads using molecular docking, fixed-bed analysis, and life cycle assessment. *Front. Chem. Eng.* 8:1887485. doi: 10.3389/fceng.2026.1887485

COPYRIGHT
© 2026 Mishra, Khare, Kumar, Banerjee, Jeon, Nayak, Chakrabortty and Tripathy. This is an open-access article distributed under the terms of the Creative Commons Attribution License (CC BY). The use, distribution or reproduction in other forums is permitted, provided the original author(s) and the copyright owner(s) are credited and that the original publication in this journal is cited, in accordance with accepted academic practice. No use, distribution or reproduction is permitted which does not comply with these terms.

Mechanistic insight into CBB-G removal by NiO@chitosan beads using molecular docking, fixed-bed analysis, and life cycle assessment

Shritee Mishra[1], Divya Khare[2], Ramesh Kumar[3]*, Shirsendu Banerjee[1], Byong-Hun Jeon[3], Jayato Nayak[4]*, Sankha Chakrabortty[1]* and Suraj K. Tripathy[1]*

[1]School of Chemical Engineering, Kalinga Institute of Industrial Technology, Bhubaneswar, India, [2]Centre for Sustainability, Mahindra University, Hyderabad, Telangana, India, [3]Department of Earth Resources & Environmental Engineering, Hanyang University, Seoul, Republic of Korea, [4]Centre for Life Science, Mahindra University, Hyderabad, Telangana, India

Introduction: In this study, the present work describes a work that analyzed the synthesis/performance of NiO@chitosan composite beads for the removal of Coomassie Brilliant Blue G (CBB-G) from aqueous systems successfully under both batch and fixed-bed conditions.

Methods: NiO nanoparticles were prepared by co-precipitation and homogenized in a chitosan matrix to generate stable, spherical beads with improved adsorption performance. XRD, FTIR, FE-SEM/EDS, BET, zeta potential, and pHpzc characterization suggested NiO incorporation and adsorption sites existed. The batch analyses have shown that the adsorption efficiency was strongly dependent on stirring speed, dosage of the adsorbent, dye concentration, pH and temperature of the sample to attain an optimum condition at 150 r/min (revolutions per minute), 54 g/L, 30 mg/L, pH 7 °C and 30 °C. For linear kinetic analysis, a pseudo second order model (R^2 = 0.9993) was used, while the equilibrium data supported Langmuir isotherm ($R^2 \approx 0.99$), confirming the dependence of monolayer adsorption on physical interactions.

Results and Discussion: In fixed-bed adsorptive investigations, breakthrough profiles were majorly dependent on bed height, inlet concentration, and feed flow velocity. The Thomas and Yoon–Nelson models with high $R^2 \approx 0.99$ corroborated significantly with experimental outcome where predictive accuracy was validated with Clark model. Thermodynamic results (ΔH° = 39.58 kJ/mol) suggested spontaneous, endothermic, and physisorption-powered adsorption. Molecular docking verified electrostatic, hydrogen bonding, and van der Waals interactions between dye and bead surface. The beads had good reusability with only minimal effect upon losses in efficiency. Life cycle analysis indicated bead synthesis exerts largest environmental burden (105 kg CO_2-eq/kg), with 6.94 kg required per m^3 treatment, leading to 852 kg CO_2-eq/m^3. Overall, the developed NiO@chitosan beads exhibited excellent adsorption performance and reusability;

however, further optimization of the synthesis process is necessary before they can be considered a fully sustainable adsorbent for large-scale wastewater treatment.

KEYWORDS

NiO@chitosan beads, Coomassie Brilliant Blue G dye removal, batch and column adsorption, kinetic modeling, molecular docking, life cycle analysis, wastewater treatment

Highlights

- NiO@chitosan beads manufactured by co-precipitation proved higher adsorption and mechanical stability for dye removal.
- This was enhanced by the best adsorption at 150 rpm, 54 g/L dosage, 30 mg/L dye, pH 7, and 30 °C, to achieve a higher CBB-G removal efficiency.
- Pseudo-second-order kinetics (R^2=0.9993) and Langmuir isotherm ($R^2 \approx 0.9900$) validate the monolayer physisorption behavior.
- Fixed-bed studies matched Thomas and Yoon–Nelson models ($R^2 \approx 0.9900$), establishing good breakthrough prediction accuracy.
- LCA yielded 852 kg CO_2-eq/m^3 impact, with 6.94 kg beads needed, suggesting opportunity for sustainable process optimization.

1 Introduction

The introduction of synthetic dyes in aquatic systems through industrial discharges impose a crucial environmental challenge in part due to their complexity in aromatic structures, chemical robustness, and resistance to biodegradation (Forgacs et al., 2004; Robinson et al., 2001). Out of these dyes, Coomassie Brilliant Blue G (CBB-G), is an abundant dye in the textile processing, biochemical staining, and pharmaceutical industries owing to its strong chromophoric properties, as well as its high solubility in water. It is regarded as an emergent organic contaminant due to its persistence in aquatic ecosystems and probable toxicological impacts. Because of its intricate aromatic structure and sulfonic acid groups, CBB-G demonstrates significant chemical stability and biodegradation resistance, enabling its persistence in wastewater and natural aquatic environments. Its presence in aquatic systems diminishes light penetration, consequently impeding photosynthesis in aquatic flora and algae, reducing dissolved oxygen concentrations, and disturbing aquatic ecosystems. In addition, CBB-G has been reported to induce cytotoxicity and oxidative stress in exposed cells and aquatic organisms at elevated concentrations. Although CBB-G is widely used as a protein-staining reagent and is generally considered to have low acute toxicity, occupational exposure through skin contact, inhalation, or accidental ingestion may pose health risks. According to available safety and toxicological studies, exposure to CBB-G can cause irritation of the skin, eyes, and respiratory tract, while inhalation of dye particles may irritate the respiratory mucosa and accidental ingestion may result in gastrointestinal discomfort. Therefore, the persistence and uncontrolled discharge of CBB-G into aquatic environments not only threaten aquatic organisms and wildlife but also increase the potential for human exposure, underscoring the need for its effective removal from industrial wastewater (Yagub et al., 2014). This is why, in light of these issues, efficient and sustainable technology of CBB-G removal has been emerging. A number of conventional processing techniques (such as coagulation–flocculation, membrane filtration, advanced oxidation processes, and biological degradation) have been examined for the removal of the dye. Nevertheless, under some circumstances such techniques have shortcomings, i.e., high cost of operation, sludge generation, membrane fouling, incomplete degradation, or strict operational requirements (CRINI, 2006). In contrast, however, adsorption is emerging as one of the potential routes due to its simplicity, cost-saving technology, quick kinetics, fast response times and for batch and continuous processes (Gupta and Suhas, 2009). The essence of successful adsorption is design of high-affinity, resistant, regenerable and stable adsorbents which have a high specific binding and regrowth adsorption against pollutant targeted molecules. Deacetylated chitin derived Chitosan, an organic biopolymer has been extensively studied as a green adsorbent because of its biodegradability, non-toxicity and presence of functional groups, such as amino (–NH_2) and hydroxyl (–OH) groups. Such characteristics can be utilized for this purpose of wastewater treatment. These functionalities allow for electrostatic interaction, hydrogen bonding and surface complexation with dye molecules. In order to improve the limitations of raw chitosan, many modification methods have been employed to enhance its mechanical stability, adsorption ability, and operation durability, such as chemical cross-linking, polymer blending or grafting, and incorporating with carbon-based nanomaterials and inorganic nanoparticles. For chemical cross-linking, chemical crosslinking agents like glutaraldehyde, epichlorohydrin and genipin could strengthen its mechanical stability and chemical stability; while excessive cross-linking would lead to lower content of amino groups used for adsorptive adsorption sites. For polymer blending, combining chitosan with materials such as alginate, cellulose and poly (vinyl alcohol) can not only improve the physicochemical properties but also processability of chitosan, but the modification involves multi-step fabrication process and might restrict the accessibility to adsorptive sites. Similarly, by incorporating carbon materials, including activated carbon, graphene oxide, carbon nanotube and biochar into chitosan can promote surface area and capacity; however the preparations typically require further functionalization, comparatively complicated fabrication processes, and high costs of manufacturing (Vakili et al., 2014). The method of embedding metal oxide nanoparticles into chitosan to simultaneously improve the structural strength, reactivity of surface and adsorptivity is an efficient way of enhancing chitosan-based adsorbents; various metal oxides, such as TiO, ZnO, FeO, CuO, MgO and AlO, are the materials widely studied and successfully applied in chitosan matrix in wastewater remediation applications (Jiang et al., 2024). The TiO-chitosan composites show the desirable photocatalytic efficiency and good stability, but usually require UV radiation to exhibit higher effectiveness (Hasmath Farzana and

Meenakshi, 2015). ZnO–chitosan composites possess high adsorption capacity and antimicrobial properties; however, their stability may be compromised under acidic conditions due to partial dissolution (Zhang et al., 2021). Fe_3O_4–chitosan composites enable convenient magnetic separation and recovery of the adsorbent, although oxidation and nanoparticle agglomeration may reduce their long-term adsorption performance (Wang et al., 2023). CuO–chitosan composites exhibit strong affinity toward various organic pollutants; however, the potential release of copper ions under certain operating conditions has raised concerns regarding secondary environmental contamination (Jiang et al., 2024). MgO- and Al_2O_3-modified chitosan composites have also demonstrated promising adsorption performance owing to their chemical stability and surface basicity, although their adsorption behaviour is highly dependent on the nature of the target pollutant and operating conditions (Jiang et al., 2024). In comparison, Nickel oxide (NiO) nanoparticles possess a high specific surface area, excellent thermal and chemical stability, abundant surface hydroxyl groups, and coordinatively unsaturated Ni^{2+} active sites that facilitate electrostatic interactions, hydrogen bonding, and surface complexation with dye molecules. Furthermore, NiO nanoparticles can be uniformly dispersed within the chitosan matrix, resulting in enhanced mechanical strength, reduced swelling, improved surface reactivity, increased availability of active adsorption sites, and excellent reusability under both batch and continuous fixed-bed operating conditions. These combined characteristics, together with the ease of synthesis and compatibility with the chitosan matrix, provide a strong rationale for selecting NiO as the reinforcing metal oxide in the present study for the development of efficient, reusable, and sustainable adsorbents for dye-contaminated wastewater treatment. The resulting NiO@chitosan composite beads offer practical advantages, including easy separation, improved hydrodynamic behaviour, reduced pressure drop, and suitability for continuous packed-bed operation (Lau et al., 2023). Beads are capable of providing practical benefits, such as easy separation, better hydrodynamic behaviors, reduced pressure drop, and potential for use with continuous packed-bed design. While various results have been published on dye removal using chitosan-based composites, comprehensive studies examining batch adsorption optimization, kinetics and isotherm modeling, thermodynamic analysis, fixed-bed column performance, and molecular level interaction are still incomplete for CBB-G adsorption. The adsorption mechanism at macroscopic as well as molecular scales underlines the importance of optimizing process parameters and predicting performance on large scale parameters. Chitosan being a emerging biopolymeric material for wastewater processing, its production and utilization can encourage a circular business model, as the beads produced can the chitosan beads have the merits of not producing secondary pollution that generally occurs due to the use petroleum-based adsorbents and resins (Shi et al., 2024; Zhao H. et al., 2021) and these can be recycled and reused for several cycles (Iqbal et al., 2025). However, evaluating the sustainability of materials requires measuring their impacts throughout the product's entire life cycle, which can be achieved through Life Cycle Assessment (LCA). Although there have been studies of chitosan composite beads, there has been an absolute lack of studies on chitosan–NiO beads in the Indian context (Iqbal et al., 2025). Hence, this study will focus on measuring the environmental impacts of chitosan-NiO beads and their use in adsorption-based clarification of dye contaminated wastewater.

In the present study, NiO nanoparticles were synthesized and incorporated into a chitosan matrix to fabricate stable NiO@chitosan composite beads for the removal of CBB-G dye. Batch experiments were conducted to evaluate the influence of stirring speed, adsorbent dosage, initial dye concentration, pH, and temperature on adsorption performance. Kinetic, isotherm, and thermodynamic analyses were performed to elucidate the adsorption mechanism (Ho and McKay, 1999a). Furthermore, fixed-bed column studies were carried out to examine breakthrough behavior under varying operational conditions, and suitable dynamic models were applied for performance prediction. Molecular docking simulations were also employed to examine the interaction between CBB-G molecules and active sites on the composite surface (Tran et al., 2017). An overall consideration of sustainability needs to be conducted on life-cycle assessment in a holistic context, as carried out via LCA. Despite the broad ranging topics and papers about chitosan-based composites, less scope of research has been paid to chitosan–NiO systems especially considering Indian context. Thus, this study will also consider the environmental evaluations related to NiO@chitosan bead manufacturing and their utilization in adsorption-based remediation of dye-contaminated wastewater, offering comprehensive evaluation of their performance and sustainability. Such integrated approach enables comprehensive understanding of the adsorption statistics of NiO@chitosan beads highlighting its potential in terms of dye removal efficiency, reusability and environmental sustainability for dye-contaminated wastewater processing.

2 Materials and methods

2.1 Raw materials and reagents

Sodium hydroxide pellets (NaOH), shrimp shell-derived chitosan, Coomassie Brilliant Blue G (CBB-G) and nickel (II) chloride hexahydrate ($NiCl_2.6H_2O$) were bought from Hi-Media Laboratories Pvt. Ltd. India. Ammonium hydroxide (NH_4OH) solutions were acquired from Sigma-Aldrich. All reagents utilized in this research were of analytical grade, with at least 99% purity, and were applied as received, without additional purification.

2.2 Preparation of NiO@chitosan beads and characterizations

NiO nanoparticles were synthesized using an improved co-precipitation approach. $NiCl_2.6H_2O$ (2.1 g, 0.5 M) was dissolved for 1–2 h in 10 mL deionized water with constant stirring (300 rpm) and ammonium hydroxide was added dropwise until pH nine to induce precipitation. The solution was aged for 12–18 h for particle stabilization followed by filtration, washing again and drying for 12 h at 60 °C–70 °C, giving $Ni(OH)_2$. The intermediate was calcined for a period of 4 h at 450 °C to prepare NiO nanoparticles. For bead preparation, 1 g chitosan was dissolved in 2% acetic acid and mixed with 4 g NiO nanoparticles under stirring for 2 h for homogeneous dispersion. The obtained mixture was transferred into 0.5 M NaOH

solution to obtain stable spherical NiO@chitosan beads, which were washed thoroughly until pH remained neutral. The synthesized materials were characterized by advanced analytical techniques. Powder X-ray diffraction (XRD) (PANalytical and Bruker, Cu Kα, λ = 1.54 Å) was used to determine the crystallinity and phase composition. Fourier transform infrared spectroscopy (FTIR) analysis (Shimadzu IR Affinity-1S and PerkinElmer Spectrum Two, ATR mode, 400–4,000 cm^{-1}) indicated that functional groups were present before and after dye adsorption. Field-emission scanning electron microscopy coupled with energy-dispersive X-ray spectroscopy (FE-SEM/EDS; Carl Zeiss Supra 55) was employed to examine the surface morphology and elemental composition of the synthesized materials. The particle size of the NiO nanoparticles was estimated from the FE-SEM micrographs using ImageJ software (National Institutes of Health, Bethesda, MD, USA). The measured particle diameters were subsequently analyzed, and the particle size distribution was plotted using Origin software (OriginLab Corporation, Northampton, MA, USA). The Brunauer–Emmett–Teller (BET) analysis (Autosorb iQ-X, 77 K) was used to reveal characteristics like surface area, pore volume and pore size distribution. Moreover, the surface charge properties and adsorption performance were analyzed by zeta potential (Anton Paar LiteSizer 500, pH 7).

To investigate the surface chemistry of NiO@chitosan beads in aqueous solution, ion adsorption method was being utilized. A number of 10 conical flasks were used, each containing amount of water of about 20 mL where the pH was adjusted between the range from 2 to 11 using NaOH or HCl solutions of desired molar concentration using pH meter of SYSTRONICS μPh System 361. Subsequently, 1 g of the sorbent was added to each flask were placed in a shaking incubator for 24 h at room temperature to reach equilibrium (Noh and Schwarz, 1989). The pH of each suspension was meticulously measured.

2.3 Adsorption procedure and break through study

Batch and continuous adsorption investigations were performed which monitored the removal of CBB-G dye using NiO@chitosan beads. For batch studies, 50 mL of the dye solution was introduced into 100 mL Erlenmeyer flasks and adsorbent was added. Flasks were mixed in a shaking incubator (Model 3016 R, Laboratory Tech, Korea) at controlled temperature conditions (Foo and Hameed, 2010). The pH of the solution was adjusted using NaOH or HCl and monitored using a Systronic pH meter (μC pH-system 361, India). The conditions including stirring speed, pH, levels of adsorbent, initial dye concentration, temperature and contact time were carefully adjusted to achieve the expected values. After adsorption, the residual dye content was determined at 585 nm on UV–Vis spectrophotometer (Cary-60, Agilent, USA). For continuous studies, fixed-bed column experiments were performed with a borosilicate glass column (R&M) with 10 mm diameter and 500 mm height at room temperature without pH adjustment. 10 mm thick layers of glass wool were applied from both sides to aid the adsorbent bed, which were packed together with NiO@chitosan beads. The dye solution was applied in a downward flow using a peristaltic pump (Cole-Parmer, USA) and waste effluent was collected periodically. Effects of bed depth (3, 6, and 9 cm of 2, 4, and 6 g adsorbent), influent concentration (3, 5 and 7 mg/L) and flow rate (10, 15, 20 mL/min) were evaluated. Dye concentration of the samples was estimated by the UV–Vis Spectroscopy (Perkin-Elmer Lambda 35, USA) at 585 nm (Bakhta et al., 2024).

The adsorption performance was then evaluated by calculating the percentage removal efficiency and the equilibrium adsorption capacity using the respective formulas (Equations 1 and 2). This systematic approach allowed for precise assessment of how different experimental conditions influenced the adsorption efficiency of NiO@chitosan beads.

$$A = \left[\frac{C_0 - C_i}{C_0}\right] \times 100 \tag{1}$$

$$q_e = \left[\frac{V\,(C_0 - C_i)}{C_0}\right] \tag{2}$$

where A represents efficacy of this adsorptive process, q_e denotes the loading at equilibrium, m is the mass of the adsorbent, V = total volume of the reaction, C_0 = initial concentration of the adsorbate, and C_i = concentration of the adsorbate at equilibrium.

Break through time and the shape of break through curve are major factors that can effectively be used to determine the efficiency of the adsorption column. The bed height, concentration and flowrate of the adsorbate are the factors involved in the shape of a fixed-bed column which determines the adsorbent affinity and adsorption pathways, is a plot of C_t/C_0 versus time t, where C_t and C_0 are the concentration at time t and at the beginning, respectively. In this work, the breakthrough time (t_b, min) was defined as the time when the outlet stream concentration reaches 5% of the influent concentration, while the saturation time (t_s, min) was taken as the duration required for the outlet stream to reach above 90% of the influent concentration (Lai et al., 2024). The treated effluent volume V_{eff} (mL), V_b (ml) and V_s (mL) can be estimated by Equations 3–5

$$V_{eff} = Q \times t_{total} \tag{3}$$

$$V_b = Q \times t_b \tag{4}$$

$$V_s = Q \times t_s \tag{5}$$

Where V_b (mL) and V_s (mL) are considered to be breakthrough and saturation volume, Q ($mL.min^{-1}$) is the feed flow rate, and t (min) can be t_{total}, the total flow time, respectively. The total CBB-G dye, q_{tot} (mg), in the column for inlet concentration of C_0 and the flow rate Q (mL/min) are obtained by integrating the plot of adsorbed concentration (C_{ad}) versus the flow time according to Equation 6

$$q_{tot} = \frac{QA}{1000} = \frac{Q}{1000}\int_{t=t_0}^{t=t_e} C_{ad}dt \tag{6}$$

The total amount of CBB-G dye delivered to the column system m_{tot} (mg) is calculated from Equation 7

$$m_{tot}\,(mg) = \frac{C_0 V_{eff}}{1000} \tag{7}$$

The equilibrium adsorption capacity, denoted as q_e and expressed in milligrams of CBB-G dye adsorbed per Gram of adsorbent (mg/g), represents the amount of CBB-G dye retained by the adsorbent at equilibrium. The difference between the

concentrations, $C_{ad} = C_0 - C_t$, corresponds to the amount of CBBG dye adsorbed. Additionally, the effective volume of the solution that has passed through the adsorption column (V_{eff}) is included in the calculation. Through the combination of these variables, rate of CBB-G dye adsorption can be evaluated the following Equation 8:

$$q_e = \frac{q_{tot}}{M} \tag{8}$$

M (g) represents the mass of the adsorbent applied in the fixed-bed column. The removal percentage R (%) of CBBG dye as follow as Equation 9

$$R(\%) = \frac{q_{tot}}{m_{tot}} \times 100 \tag{9}$$

The equilibrium concentration (C_e) was calculated using the expression (Equation 10)

$$C_e = \frac{m_{total} - q_{total}}{V_{eff}} \times 1000 \tag{10}$$

2.4 Reusability and ecotoxicological study

The dye-loaded NiO@chitosan beads were separated from the solution by filtration following each adsorption experiment. The recovered beads were washed three times with distilled water to remove loosely bound or residual dye molecules and subsequently dried at room temperature until completely dry. The washed and dried beads were then reused under the same optimized experimental conditions in subsequent adsorption cycles to evaluate their reusability and adsorption stability (Boricha and Murthy, 2010). CBB-G dye is an essential staining agent in biochemical and molecular biology studies; however, for environmental persistence and potential adverse impacts on aquatic ecosystems, the need for proper treatment is reinforced by the necessity of its disposal practice. Agar well diffusion technique was used to evaluate the toxicity of treated waters for CBB-G dye. *Escherichia coli* (*Escherichia coli*) was used as a test microorganism and the toxicity results were compared with control samples of deionized water and water contaminated with CBB-G dye. Bacterial cultures were aerobically incubated in sterilized nutrient medium at 37 °C for 20 h using a shaker incubator. To adjust the concentration to fewer than one million cells per milliliter, the culture was diluted with a 0.9% saline solution. A sterile cotton swab was then used to uniformly spread the bacterial suspension onto nutrient agar plates. Specific volumes of CBB-G dye solution, treated water, and deionized water were dispensed into the wells created in the agar plates. After overnight incubation at 37 °C, the inhibition zones surrounding the wells were measured and analyzed. Each experiment was performed in triplicate for accuracy, and the average value from the three replicates was recorded.

2.5 Molecular docking methodology

To elucidate the adsorption mechanism of CBB-G dye on the NiO@chitosan beads at the molecular level, molecular docking simulations were carried out using the Adsorption Locator module implemented in BIOVIA Materials Studio 2020. In the adsorption model, the CBB-G dye molecule was treated as the adsorbate (ligand), while the NiO@chitosan composite was employed as the adsorbent (receptor) to investigate the intermolecular interactions governing the adsorption process. Two surface models were constructed to represent the adsorbent: (i) the overall optimized NiO@chitosan bead structure and (ii) a cleaved surface along the (111) crystallographic plane, selected for its chemical activity and energetic stability. The exposed surface is enriched with hydroxyl and amino functionalities from chitosan, together with oxygen-rich sites from NiO, which were considered potential adsorption sites during the docking simulations. During docking simulations, the adsorbent framework was constrained and maintained as a rigid body to preserve its structural integrity, whereas the CBB-G dye molecule was allowed conformational flexibility to enable effective surface accommodation. Prior to docking, both the adsorbent surfaces and the dye molecule were subjected to energy minimization using a molecular mechanics force field to eliminate steric clashes and achieve stable geometries. The molecular structure of CBB-G was retrieved from a validated chemical database and further optimized to ensure that the lowest-energy conformation was employed in docking calculations. Docking simulations were conducted using a Monte Carlo simulated annealing protocol, which facilitates extensive sampling of possible adsorption sites and orientations through random translational, rotational, and regrowth movements of the dye molecule across the adsorbent surface. A total of 100,000 loading steps were applied, followed by three annealing cycles of 15,000 steps each, after which geometry optimization was performed to ensure convergence toward energetically favourable adsorption configurations. Intermolecular interactions were described using the Universal Force Field (UFF), with atomic charges assigned according to the default "use current" scheme (Rappe et al., 1992). Electrostatic interactions were evaluated using a group-based summation method, while van der Waals interactions were calculated using an atom-based summation approach with a cutoff distance of 12.5 Å. Multiple adsorption configurations were generated during the simulations, and the most stable dye–adsorbent complexes were selected based on minimum docking interaction energy and overall energy distribution. The optimized docking configurations were further analyzed to identify the dominant non-covalent interactions responsible for adsorption stability, including electrostatic attraction, hydrogen bonding, and van der Waals interactions between the functional groups of CBB-G and the oxygen- and nitrogen-rich sites on the NiO@chitosan surface. Comparative analysis of the whole bead surface and the (111) plane provided molecular-level insights into the preferred adsorption sites and stabilization mechanisms governing CBB-G uptake. A schematic representation of the docking workflow and interaction pathways is provided in Figure 1.

2.6 Methodology of life cycle assesment (LCA)

The LCA following the ISO 14040 methodology was conducted using the openLCA software with the Ecoinvent 3.11 database, and the impact assessment method used was ReCiPe 2016 v1.03 (H) for evaluating impacts using the midpoint method. This method was chosen because it includes a range of impact categories and can convey the uncertainty of the model (Bisaria et al., 2024). The goal of

10.3389/fceng.2026.1887485

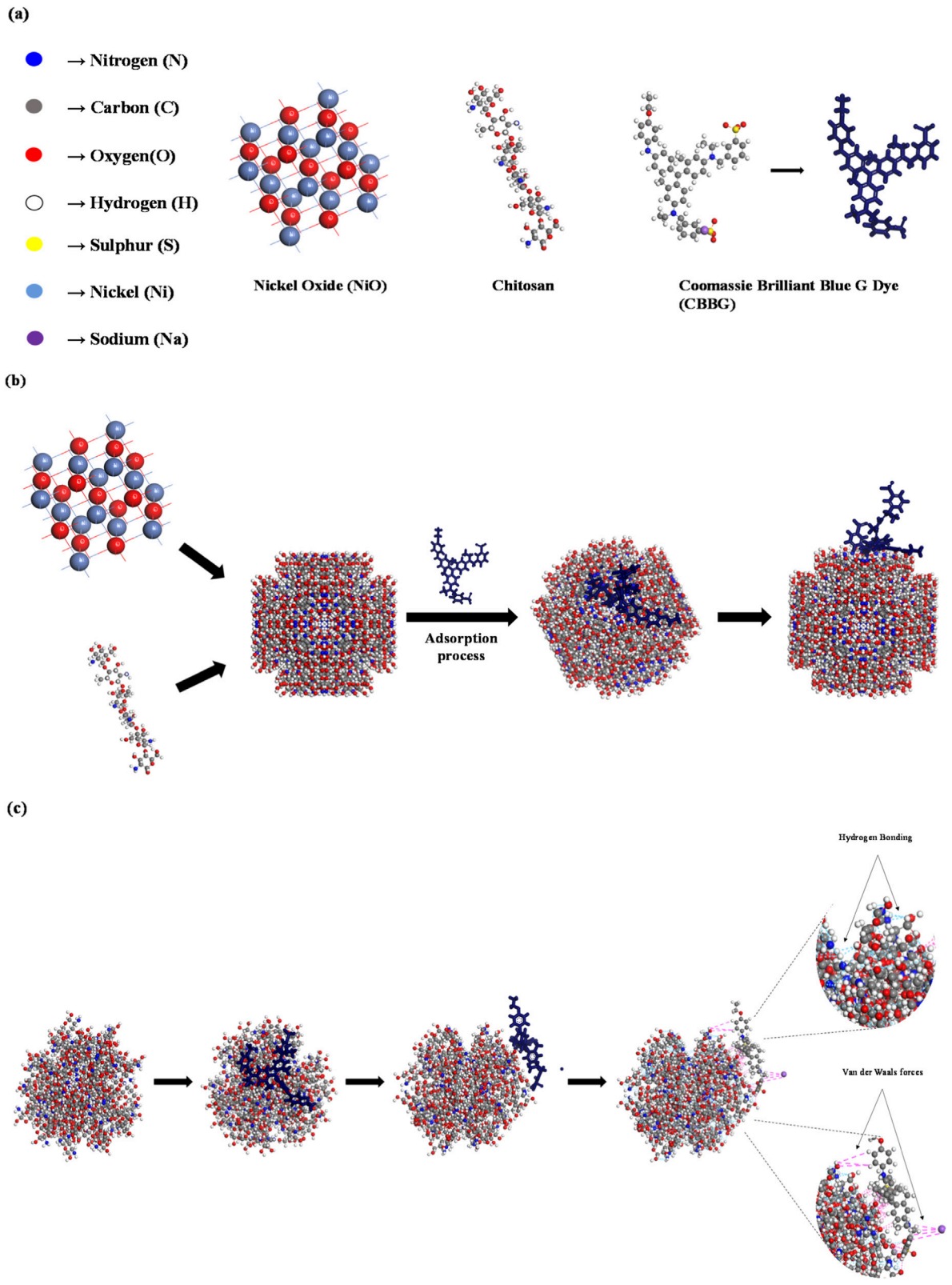

FIGURE 1
Molecular docking analysis of CBBG adsorption on NiO@chitosan beads: **(a)** structural models of NiO, chitosan, and CBBG; **(b)** adsorption configuration on the porous composite surface showing preferential dye anchoring within surface cavities; **(c)** interaction mechanism on the NiO (111) plane highlighting electrostatic, hydrogen bonding, and van der Waals contributions to adsorption stability.

the study is to assess the environmental impacts of Chitosan-NiO beads across its life cycle. Two lifecycles were conducted with varying system boundaries (Figure 2). One was focused exclusively on bead production (gate-to-gate), while the other one was targeted on its application in treatment of dye infected wastewater and its clarification process in an adsorption column. For the later one, system boundary was extended to encompass the application phase, providing a more comprehensive view of the product's environmental performance. Performing two separate Life Cycle Assessments (LCAs) with different system boundaries allows a more granular understanding of where environmental burdens occur. The life cycle assessment was conducted based on several modelling assumptions. The background production of $NiCl_2.6H_2O$ was represented using a proxy dataset from ecoinvent v3.11, modelling the electricity consumption with background process like the Indian electricity mix–Eastern Grid from ecoinvent 3.11, the beads reuse was considered to be four times and the chitosan production was excluded from the study as it was beyond the scope of the study (as laboratory grade reagent was used during the process).

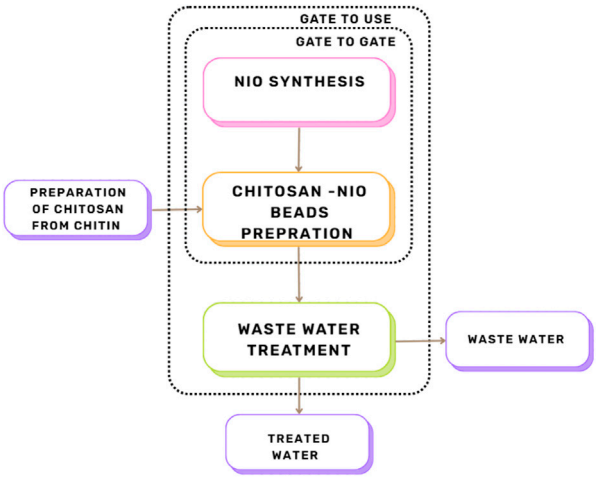

FIGURE 2
System boundaries diagram representing the two scopes considered in this study within the same process.

3 Result and discussion

3.1 Materials characterization

XRD analysis (Figure 3a) confirmed the crystalline NiO phase of NiO@chitosan beads, which were characterized by well defined peaks at 2θ = 37.27°, 43.24°, 62.99°, 75.54°, and 79.44° for the (111) (200), (220), (311), and (222) planes, in agreement with JCPDS standards, and suggesting a face-centered cubic structure (Rathika et al., 2024). According to previous reports, pure chitosan typically exhibits two broad diffraction peaks at approximately 2θ = 10° and 20°, characteristic of its semi-crystalline structure. The emergence of distinct NiO diffraction peaks in the present composite, together with the reduced contribution of the characteristic chitosan reflections, confirms the successful incorporation of crystalline NiO into the chitosan matrix and the resulting modification of its crystallinity (Morsy et al., 2019; Pham et al., 2022). FTIR spectra (Figure 3b) highlighted important functional groups, including Ni–O (669 cm^{-1}), C=O (1,653 cm^{-1}) and N–H (1,584 cm^{-1}). However the peak shifts (1,653→1,638 cm^{-1}; 1,584→1,580 cm^{-1}) and band broadening after adsorption confirmed that dye molecules bind to active sites by hydrogen bonding and electrostatic forces (Pham et al., 2022; Alhumaimess et al., 2025). BET analysis (Figures 3c,d) shown mesoporous structure with a specific surface area of 34.56 m^2/g and average pore diameter of 12.29 nm, promoting adsorption via capillary condensation and improving surface accessibility (Wang and Peng, 2010). Zeta potential was −10.6 mV and close to neutral to slightly negative, whereas the point of zero charge (Figure 3e) was 7.75, indicating a surface charge reversal near neutral pH (Qi et al., 2004). Despite the negative surface charge, the adsorption of anionic CBB-G dye occurs through hydrogen bonding, van der Waals interactions and potentially coordination with Ni^{2+} sites. The maintained signals of Ni–O and chitosan backbone show structural integrity, whereas mesoporosity, particle localization at nanoscale scales, and multifunctional surface groups lead to promoted adsorption performance. The figure (Figure 3f) shows the determination of the point of zero charge (pHpzc) of the NiO@chitosan beads using a ΔpH versus initial pH (pH_i) plot. An obvious decreasing gradient is noted where ΔpH changes with respect to pH_i increasing from positive to negative values, showing concomitant change of surface charge patterns. The point of intersection at ΔpH = 0 is at approximately pHpzc ≈7.75. This suggests that the adsorbent surface is positively charged at pH values below 7.75 and becomes negatively charged above this value. The electrostatic attraction between the positively charged surface and the negatively charged dye molecule should enhance adsorption under acidic conditions since CBB-G is an anionic dye with sulfonate ($–SO_3^-$) groups. However, this large adsorption in the vicinity of neutral pH indicates that hydrogen bonding, van der Waals forces, and possible co-contribution of Ni^{2+} sites are another determinant of adsorption. Therefore, the pHpzc result confirms that adsorption behavior is in part a combination of electrostatic and physicochemical interactions and not only a charge-dependent effect.

The FE-SEM images (Figures 4a–f) revealed uniformly distributed spherical NiO@chitosan beads with rough and porous surfaces. High-magnification images showed well-dispersed NiO nanoparticles (20–35 nm) embedded within the chitosan matrix, providing a high active surface area for adsorption. After adsorption, the bead surface appeared comparatively smoother and partially covered by a deposited dye layer, indicating the occupation of the available adsorption sites by CBB-G molecules. The corresponding EDS spectra (Figures 4g,h) further confirmed the adsorption process. Before adsorption, the spectra were dominated by carbon (C), oxygen (O), and nickel (Ni), which are characteristic of the chitosan matrix and NiO nanoparticles. After adsorption, a distinct sulfur (S) peak appeared due to the sulfonate ($–SO_3^-$) groups present in the CBB-G dye molecules, together with slight changes in the relative intensities of the C, O, and Ni peaks caused by surface coverage of the adsorbent by the adsorbed dye. These changes in surface morphology and elemental

10.3389/fceng.2026.1887485

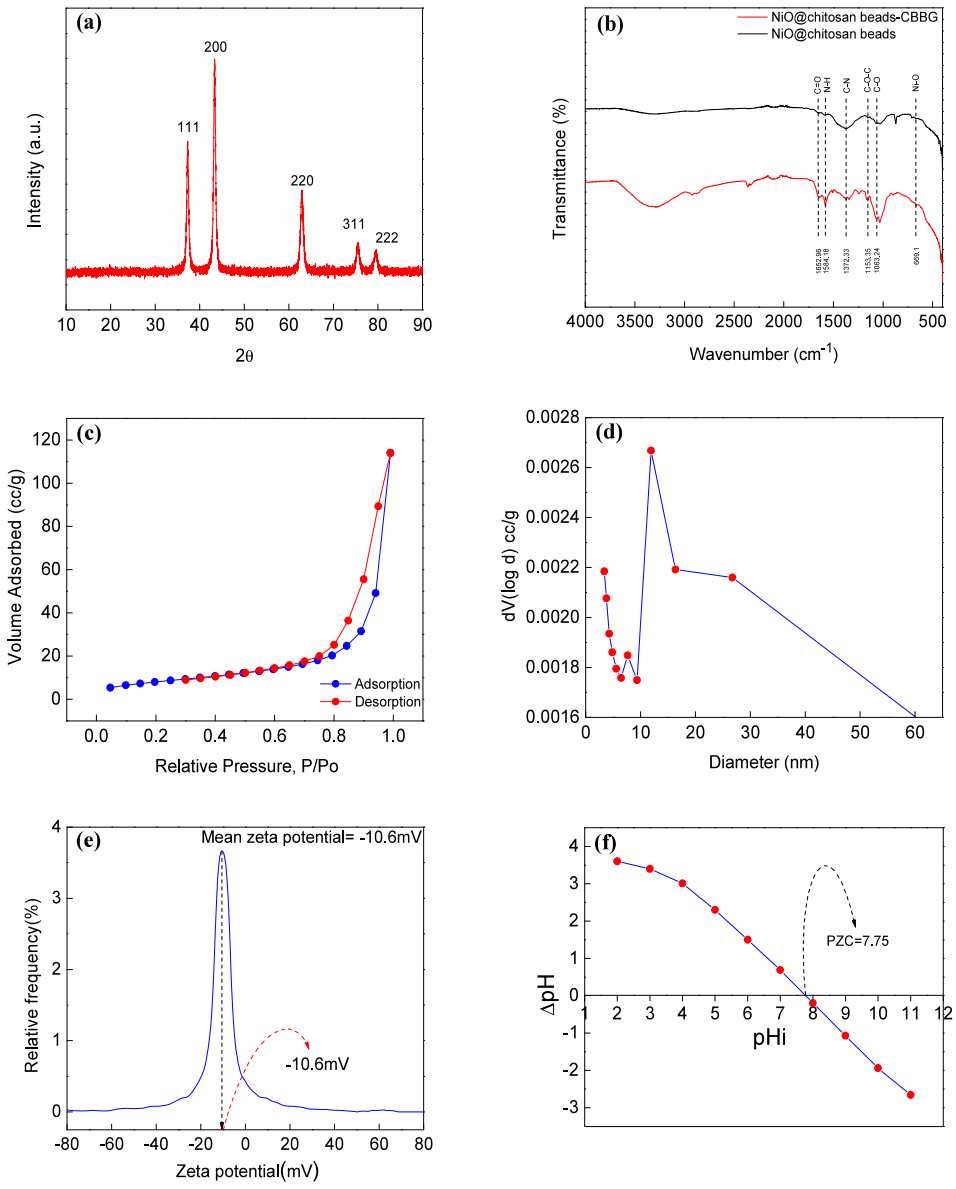

FIGURE 3
(a) XRD diffraction pattern, **(b)** FTIR spectra, **(c)** BET, **(d)** particle size distribution curve **(e)** Zetapotential and **(f)** PZC of NiO@chitosan beads.

composition provide strong evidence for the successful adsorption of CBB-G onto the NiO@chitosan beads without noticeable structural deterioration (Kannan et al., 2020; Salleh et al., 2011). Particle size analysis (Figure 4i) revealed an average NiO nanoparticle size of approximately 28 nm, with most particles distributed within the 25–35 nm range. The particle size distribution exhibited an approximately Gaussian profile, indicating relatively uniform particle formation with limited agglomeration. Such a narrow particle size distribution is advantageous because smaller and uniformly dispersed nanoparticles provide a higher specific surface area and greater availability of active adsorption sites. The incorporation of these nanosized NiO particles into the chitosan matrix is expected to enhance dye diffusion and facilitate efficient interaction between the adsorbent surface and CBB-G molecules, thereby contributing to the improved adsorption performance of the NiO@chitosan beads.

3.2 Effect of operational parameters on CBB-G removal efficiency: batch and column study

For batch adsorption we varied major operating parameters, including the stirring speed, the adsorbent dose, the initial dye concentration, pH, and temperature (Figures 5a–e). The adsorption efficiency (A_e, %) was used to evaluate the removal performance of CBB-G, where A_e denotes the percentage removal of the dye from the aqueous solution. The increased stirring rate, from 50 to 250 r/min, decreased the adsorption efficiency, because of the reduced interaction time and the boundary layer effect; therefore, 150 r/min

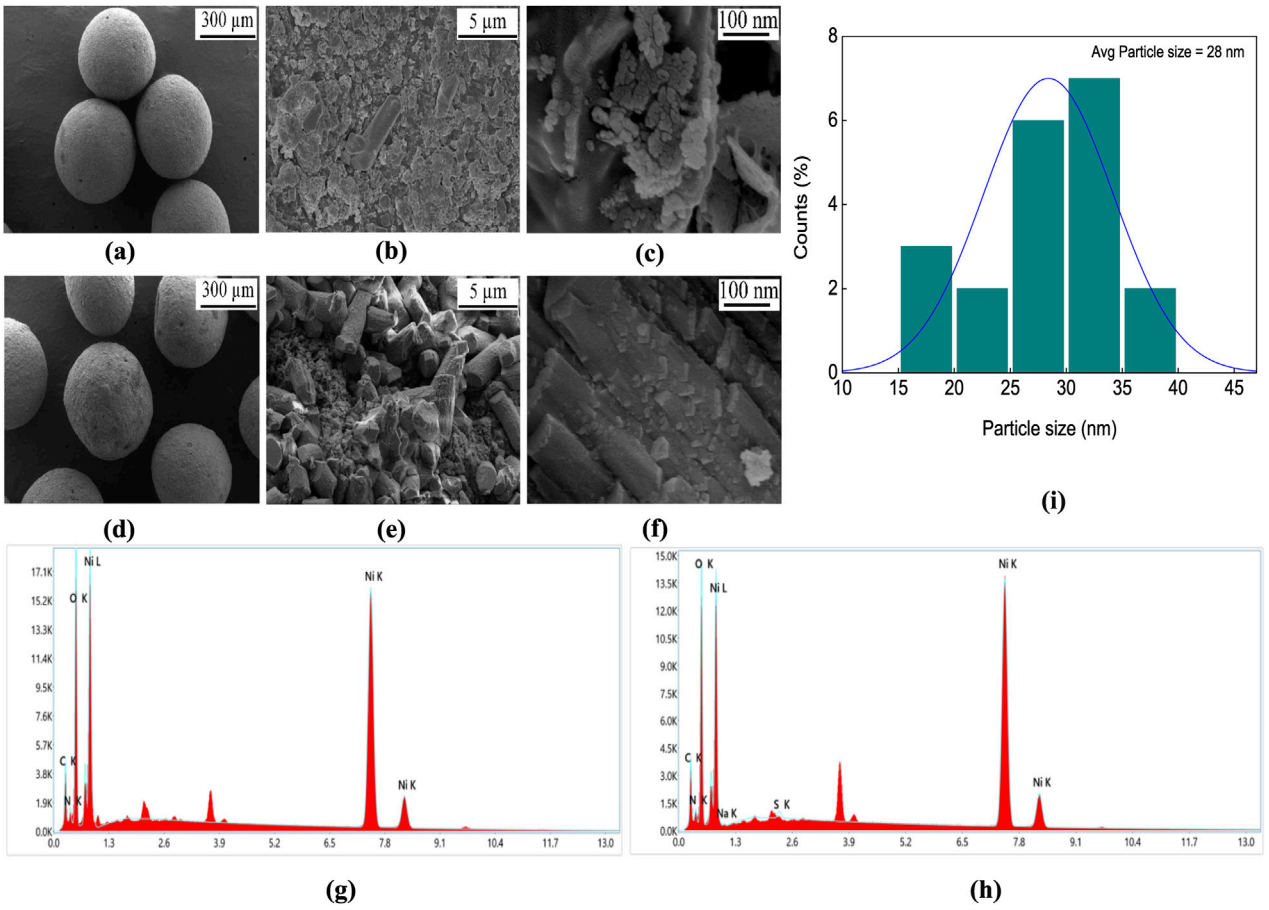

FIGURE 4
(a) FE-SEM image of NiO@chitosan beads before adsorption showing spherical morphology. **(b)** Higher magnification FE-SEM image showing rough surface texture. **(c)** High-resolution FESEM image showing embedded and agglomerated NiO@chitosan beads. **(d)** FE-SEM image of NiO@chitosan beads after CBBG adsorption **(e)** Nanoscale FE-SEM image indicating pore filling and masking of NiO@chitosan beads after adsorption. **(f)** Magnified FE-SEM image showing surface coverage after adsorption. **(g)** EDS spectrum of NiO@chitosan beads before adsorption. **(h)** EDS spectrum after dye adsorption. **(i)** Particle size distribution of NiO@chitosan beads.

was determined as a ssuitable solution (Raval et al., 2017). Adopting the adsorbent dosage (30–84 g/L), an effective dye removal capability was observed due to a greater number of active sites formed, with an optimum rate being 54 g/L, after which q_e, caused by aggregation, attenuated substantially. At 10–50 mg/L the first-stage dye adsorption became inefficient due to site competition, and 30 mg/L was determined as an optimal concentration (Shang et al., 2016). Adsorption was enhanced by pH, therefore pH seven was selected based on pHpzc (7.75), suggesting good electrostatic relationship between dye molecules and the adsorbent surface (Raval et al., 2017). Temperature up to 30 °C–45 °C resulted in better adsorption, verifying the endothermic nature of the process because of higher molecular mobility and diffusion. Adsorption was found to be strongly impacted by bed height, influent concentration, and flow rate in the fixed bed column tests (indicated in Figures 6a–c). Increasing bed height of the column from 3 to 9 cm resulted in higher breakthrough time (10–66 min) and achieved removal efficiency of 53.54%–68.25% due to increased contact time and the presence of more adsorption sites (Arulkumar et al., 2011). The increase of influent concentrations (3–7 mg/L) showed that the breakthrough was even earlier (22–6 min) indicating faster saturation, whereas 5 mg/L optimized, which provided an appropriate balance between removal efficiency and adsorption capacity (Kjidaa et al., 2023). Additionally, breakthrough time (10–30 mL/min) was observed to decrease from 10 to 2 min when flow rate was increased due to insufficient residence time, with 10 mL/min identified as optimal (Kjidaa et al., 2023). These measurements show that the performance is controlled by the mass transfer dynamics and operating environment and serve as a good basis for further system optimization and upscaling.

To elucidate the contribution of NiO to the adsorption process, the adsorption performance of pure chitosan beads was compared with that of NiO@chitosan beads under identical experimental conditions (Supplementary Figure S5). The UV–Vis spectra showed that pure chitosan beads gradually reduced the characteristic absorbance peak of CBB-G at approximately 585 nm, achieving a maximum dye removal efficiency of nearly 72% after 180 min. In contrast, NiO@chitosan beads exhibited a substantially greater decrease in absorbance, achieving nearly 99% dye removal under the same conditions. The incorporation of NiO therefore enhanced the removal efficiency by 27% points, demonstrating its significant contribution to the adsorption

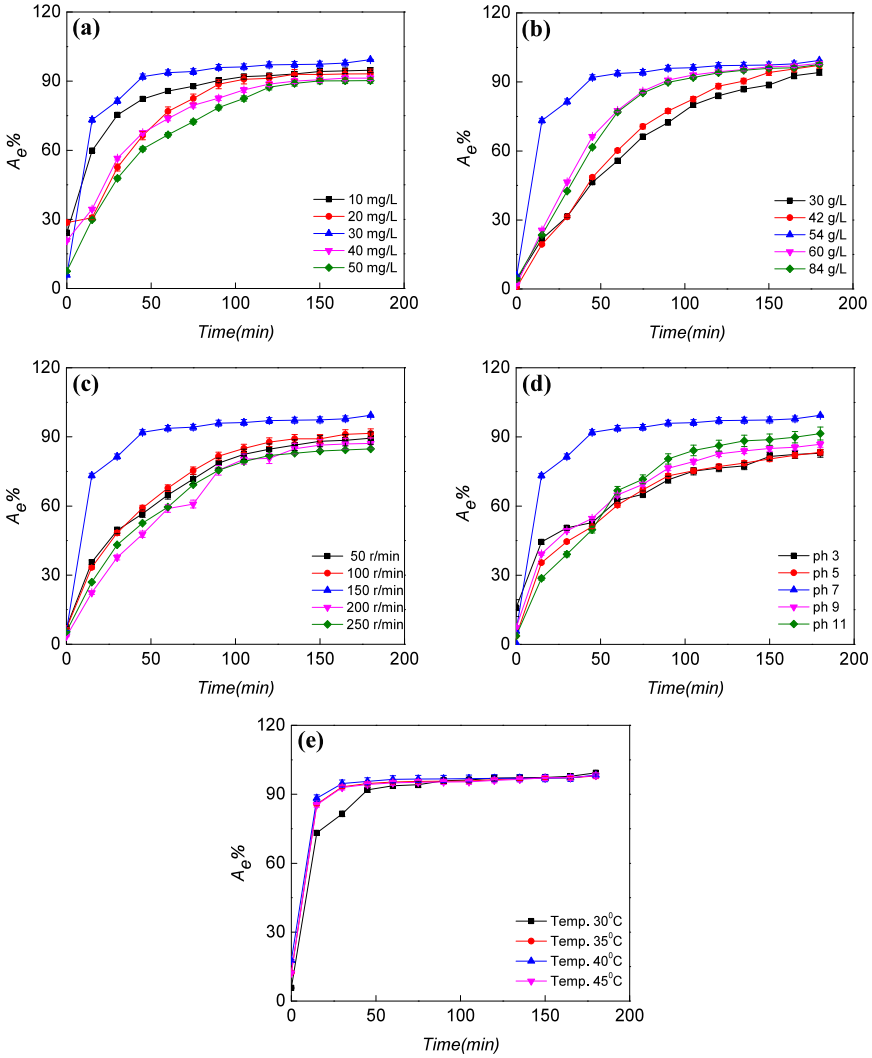

FIGURE 5
Process parameters **(a)** effect of concentration of dye solution, **(b)** effect of adsorbent dose, **(c)** effect of stirring speed, **(d)** effect of pH and **(e)** effect of temperature using batch adsorption.

process. This improvement can be attributed to the additional active adsorption sites provided by NiO nanoparticles and the synergistic interaction between NiO and the hydroxyl and amino functional groups of chitosan, which facilitate electrostatic interactions, hydrogen bonding, and surface complexation with CBB-G molecules.

3.3 Theoretical model analysis for batch study and column study

Supplementary Figure S2 displays the schematic models of adsorption that visualize the removal of CBB-G dye on NiO@ chitosan beads under batch and column conditions. Based on this, kinetic models of rate-controlling adsorption appear in the figure, and equilibrium isotherm models of the interaction between the dye molecules and the adsorbent surface are depicted. Dynamic column models are also illustrated for the breakthrough behavior and mass transfer characteristics of continuous systems. This integrated modeling framework gives an organized way to correlate experimental data with the adsorption mechanism and develop insight into equilibrium and dynamic adsorption processes. Supplementary Figure S3 shows linear and non-linear fitting of adsorption isotherm models for CBB-G adsorption on NiO@ chitosan beads. The linear shapes are Langmuir (a), Freundlich (b), Temkin (c), Dubinin–Radushkevich (d) models, while the non-linear expressions are shown in (e–h). The Langmuir model describes monolayer adsorption on a homogeneous surface with a finite number of active sites, and the Freundlich model describes heterogeneous surface interactions. The Temkin model incorporates adsorbate–adsorbent interactions and adsorption heat variation, and the Dubinin–Radushkevich model adds detail to adsorption energy and mechanism. In essence, comparison between linear and non-linear models allows for better parameter estimation as well as model validation, and leads to the conclusion that adsorption on NiO@chitosan beads is due to surface heterogeneity and mainly physical interactions. Supplementary Table S1 summarizes the equilibrium parameters derived from linear and non-linear fitting of Langmuir, Freundlich, Temkin and Dubinin–Radushkevich

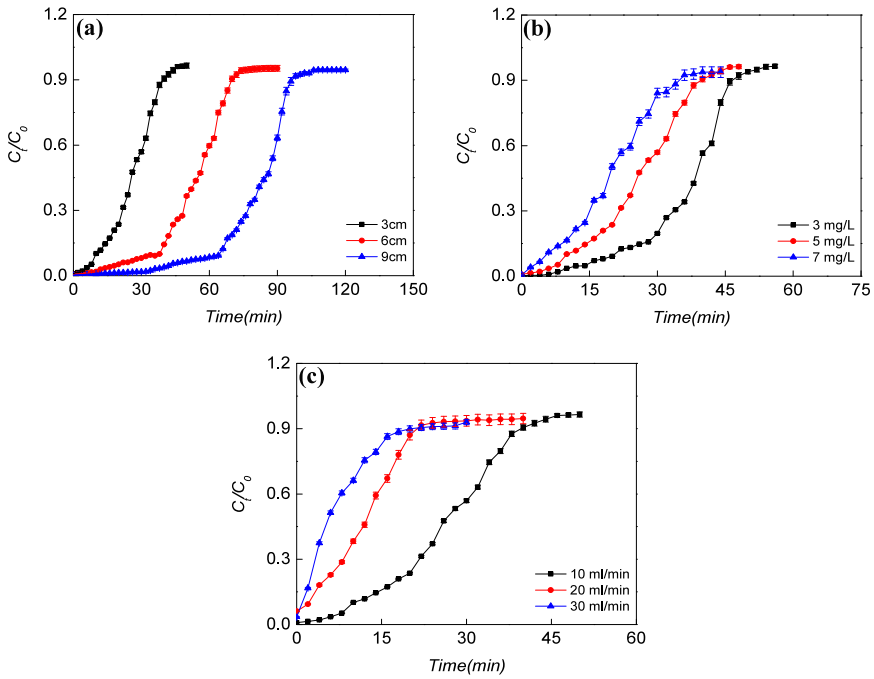

FIGURE 6
Breakthrough curves (C_t/C_0 vs. time) for CBB-G adsorption onto NiO@chitosan beads under varying **(a)** bed heights (3, 6, and 9 cm), **(b)** initial dye concentrations (3, 5, and 7 mg/L), and **(c)** flow rates (10, 20, and 30 mL/min).

isotherm models for CBB-G adsorption on NiO@chitosan beads. These parameters offer information regarding adsorption capacity, surface heterogeneity, interaction energy, and adsorption mechanism. A comparison between the linear and non-linear fitting approaches revealed that the fitting performance varied depending on the adsorption isotherm model. For the Langmuir, Freundlich, and Dubinin–Radushkevich models, the linear fitting produced slightly higher correlation coefficients (R^2 = 0.9912, 0.9796, and 0.9583, respectively) than the corresponding non-linear fitting. In contrast, the Temkin model showed improved agreement with the experimental data using the non-linear approach (R^2 = 0.9954), indicating that non-linear regression better represented the adsorbate–adsorbent interactions and the variation in adsorption heat. Although differences were observed in the estimated model parameters, both fitting approaches consistently identified the Langmuir isotherm as the most appropriate model for describing CBB-G adsorption onto NiO@chitosan beads, suggesting predominantly monolayer adsorption on a relatively homogeneous surface. These findings demonstrate that the choice of fitting approach influences parameter estimation, while the overall interpretation of the adsorption mechanism remains unchanged.

To further evaluate the adsorption performance of the developed NiO@chitosan beads, the maximum adsorption capacity was compared with those of previously reported adsorbents for the removal of CBB-G dyes, as summarized in Supplementary Table S2 while natural agalmatolite, acid-treated agalmatolite, and α-chitin nanoparticles showed adsorption capacities of 11.29, 9.84, and 8.55 mg/g, respectively (de Sales et al., 2013; Dhananasekaran et al., 2016) whereas Oyster shell-derived hydroxyapatite microspheres and Fe_3O_4 magnetic nanoparticles demonstrated considerably higher adsorption capacities of 83.82 and 124.33 mg/g (Mahmad Rozi et al., 2023; Wang et al., 2022). In contrast, Purolite A420S anion-exchange resin exhibited a comparatively lower adsorption capacity of 5.17 mg/g (Karakaya et al., 2026). The NiO@chitosan beads developed in the present study achieved a Langmuir adsorption capacity of 15.19 mg/g, which is higher than those of natural agalmatolite, acid-treated agalmatolite, α-chitin nanoparticles, and the Purolite A420S anion-exchange resin. Although the adsorption capacity is lower than that reported for oyster shell-derived hydroxyapatite microspheres and Fe_3O_4 magnetic nanoparticles, these highly engineered adsorbents generally involve more complex synthesis procedures or specialized materials. The enhanced adsorption performance of the NiO@chitosan beads can be attributed to the synergistic incorporation of NiO nanoparticles within the chitosan matrix, where the hydroxyl and amino functional groups of chitosan, together with the active sites provided by NiO, promote electrostatic interactions, hydrogen bonding, and surface complexation with CBB-G molecules. Furthermore, adsorption capacity alone should not be considered the sole criterion for evaluating adsorbent performance, as factors such as adsorbent preparation, operating conditions, adsorption kinetics, regeneration potential, cost, and applicability under continuous-flow conditions also influence practical performance. In addition to its favorable adsorption capacity, the developed NiO@chitosan beads offer several practical advantages, including a simple synthesis route, the use of biodegradable chitosan as the supporting matrix, and applicability in both batch and fixed-bed column systems. Moreover, unlike the previous studies summarized in Supplementary Table S2, the present work integrates batch

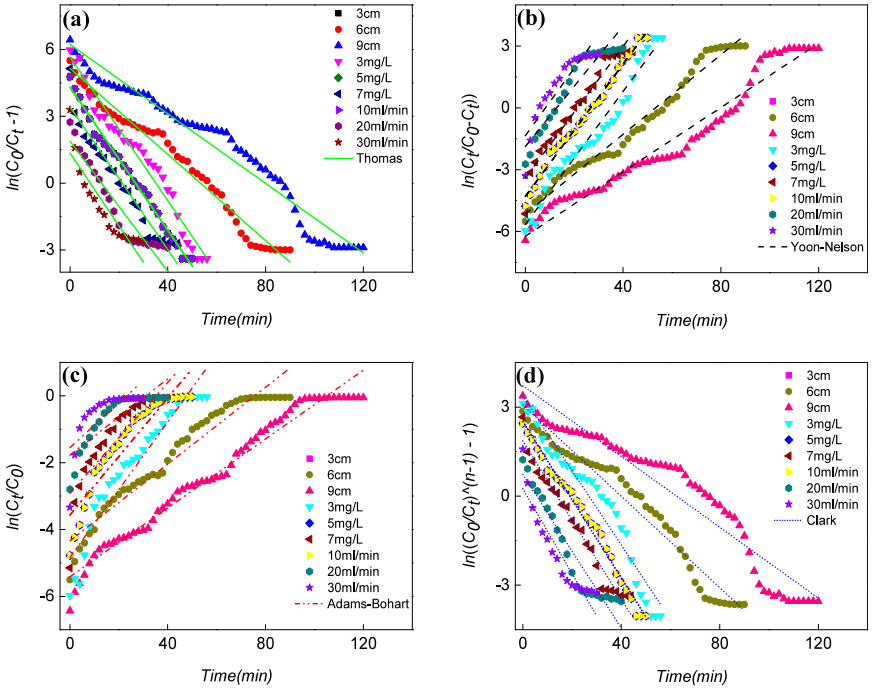

FIGURE 7
Linearized column kinetic model plots for CBB adsorption onto NiO@chitosan beads: **(a)** Thomas model, **(b)** Yoon–Nelson model, **(c)** Adams–Bohart model, and **(d)** Clark model under different operating conditions.

adsorption experiments, fixed-bed column studies, molecular docking analysis, and life cycle assessment (LCA), thereby providing a comprehensive evaluation of adsorption performance, adsorption mechanism, practical applicability, and environmental sustainability.

In batch adsorption studies the kinetics of adsorption measures the increase and decrease of adsorbate utilized by the adsorbent over time in order to pinpoint the mechanisms and rate-controlling processes that push it towards equilibrium. These studies offer fundamental analysis results of mass transfer behavior, system dynamics, and overall process efficiency factors at optimization and scale up. To estimate those issues, four commonly used kinetic models are employed: the pseudo-first-order, pseudo-second-order, intraparticle diffusion, and Elovich models (Ho and McKay, 1998). The pseudo-first order model relates the rate toward adsorption to the number of available sites; it is generalizable to physisorption especially from the initial stages. For chemically-controlled reactions, a pseudo-second-order model is superior as it also explains the square of the unoccupied sites and chemisorption: via electron sharing or transfer. The intraparticle diffusion model proposes a sequential effect of diffusion over the porous substrate from fast surface diffusion to slow-speed diffusion into the pores (Weber and Morris, 1963) and the slope and intercept of the $\sqrt{t}$ plot show an apparent heterogeneity of diffusion effects from boundary-layer influences compared to the other sources. The Elovich model is ideal for adsorption of heterogeneous surfaces because as the active sites are filled and the surface energy changes, the rate goes down exponentially.

The Thomas model was applied for column studies to estimate fixed-bed adsorption behaviour under continuous flow, assuming Langmuir kinetics and negligible axial dispersion. By making use of breakthrough data, the estimation of adsorption capacity and rate constants can support system design and optimization. The Yoon-Nelson model allows to obtain insight into the shape of breakthrough curves in an easier and more generalized way than using discrete adsorbent properties, hence minimizing errors at both early and late breakthrough stages (Yoon and Nelson, 1984). The Clark model combines the Freundlich isotherm with mass-transfer principles to describe heterogeneous systems, to instantiate full breakthrough curves, and to obtain the adsorption capacity at different points. The governing equations for the Thomas, Yoon–Nelson, and Clark models are shown in Figures 7a–d, complementing the descriptive text and offering a concise reference for interpreting adsorption performance, mechanisms, and overall system behaviour in practical applications (Podoll et al., 1987). The beneficial information that adsorption kinetics may provide concerning the mechanism of action and rate-limiting phase can further clarify the potential of the changed process parameters. The kinetic information for adsorption of CBB-G on NiO@chitosan beads is found in Supplementary Table S3. For identifying the kinetics of CBB-G dye adsorption on NiO@chitosan beads, the optimal values were an adsorbent weight of 54 g/L, a temperature of 30 °C, a CBB-G dye solution of 30 mg/L, and a stirring speed of 150 r/min. The linear plots of the $\log(q_e \rightarrow q_t)$ vs. t of the pseudo-first-order reaction and t/q_t vs. t of the pseudo-second-order reaction for using CBB-G for the adsorption on NiO@chitosan beads are shown in Supplementary Figure S4. Plotting were examined to investigate the rate parameters (Y.-S. Ho, 2006). Comparison with pseudo-second order rate (R^2 = 0.9993), Elovich (R^2 = 0.9256), intra-particle diffusion (R^2 = 0.7865) and

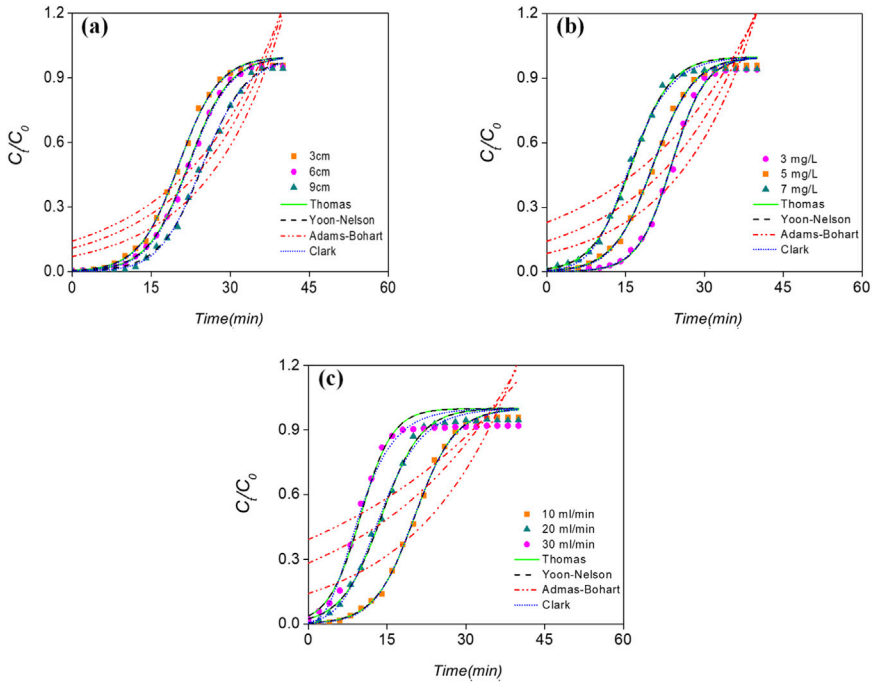

FIGURE 8
Comparison of experimental breakthrough curves with model predictions (Thomas, Yoon–Nelson, Adams–Bohart, and Clark models) under varying **(a)** bed heights, **(b)** initial dye concentrations, and **(c)** flow rates.

pseudo-first order rate (R^2 = 0.9620) show that correlation coefficient values were closer to unity for pseudo-second order rate model. Such adsorbate species may be transferred from the bulk of the solution into the solid phase by the intraparticle diffusion/transport mechanism, often rate-limiting in many adsorption processes. One important mechanism is intra-particle diffusion, which drives adsorption, although hardly the only one. The intraparticle diffusion model with a moderate fit is analyzed, with a value of (R^2 = 0.7865).

The adsorption performance of the fixed-bed column system was examined using four kinetic models: Thomas, Yoon-Nelson, Adams-Bohart, and Clark, under different experimental conditions. Among these, the Thomas model consistently achieved the highest correlation coefficient (R^2 = 0.9900) across most test cases, indicating its suitability for predicting breakthrough behaviour in the adsorption process (El-Dossoki et al., 2024). At a dye concentration of 7 mg/L and flow rate of 10 mL/min, the maximum adsorption capacity q_0 = 0.719 mg/g was obtained and gradually reduced with increase in the flow rate and initial concentration. The Yoon-Nelson model also showed good agreement with experimental data with R^2 values, showing 0.9900 in non-linear fitting. τ (breakthrough time constant) changed with bed height and influent concentration to 79.78 and 83.61 min, respectively, for linear fitting (9 cm bed height) and non-linear fitting, as summarized in Supplementary Table S5. Conversely (Figures 8a–c) the Adams-Bohart model not only performed adequately in the initial phase of the breakthrough curve, but also resulted in lower correlation coefficients than expected (R^2 between 0.5 and 0.9) for the whole curve, indicating a less reliable fit (Aksu and Gönen, 2004). The Clark model's nonlinear approach provided considerable correlation (R^2 = 0.9900), validating its relevance for modeling dye adsorption under certain operating conditions. The model fitting results clearly revealed that operational characteristics such as bed height, concentration of the influent dye, and column flow rate affect column performance. From 3 cm to 9 cm height of the bed, the adsorption capacity increased, and the breakthrough of adsorption was delayed by the expansion of the contact time and the larger adsorption sites available. On the other hand, the higher amount of flow rates like 30 mL/min led to a higher break and drop in the adsorption rate given the lower residence time which not only retarded the mass transfer between dye molecules and adsorbent (Ahmad and Hameed, 2010). The Clark model described adsorption behavior for controlled concentrations of dye and ideal bed height well and that of Thomas and Yoon-Nelson under continuous conditions for the simulation with high correlation coefficients for all the tests tested. Moreover, non-linear regression analysis had superior statistical fit than either linear model, which emphasizes the importance of non-linear analyses during column adsorption data interpretation. These results would indicate maximum dye removal efficiency and breakthrough performance in column systems and the maintenance of moderate flow rates, high bed depth and low influent concentration is critical to enhance the practical applicability of system in wastewater treatment process.

3.4 Proposed adsorption mechanism based on experimental findings

Based on the kinetic, equilibrium, thermodynamic and physicochemical characterization results, a plausible adsorption

mechanism for the removal of CBB-G by NiO@chitosan beads is proposed. The adsorption kinetics were analysed using the pseudo-first-order, pseudo-second-order, intraparticle diffusion and Elovich models, among which the pseudo-second-order model exhibited the highest correlation coefficient (R^2 = 0.9993), indicating that the adsorption rate is primarily governed by the availability of active adsorption sites on the adsorbent surface (Ho and McKay, 1999; Plazinski et al., 2009). Although the intraparticle diffusion model contributed to the adsorption process (R^2 = 0.7865), its relatively lower correlation coefficient suggests that pore diffusion was not the sole rate-controlling step, and that external mass transfer and surface adsorption also participated in the overall adsorption process (Weber and Morris, 1963; Plazinski et al., 2009). The equilibrium behaviour was investigated using Langmuir, Freundlich, Temkin and Dubinin–Radushkevich isotherm models. Among these, the Langmuir model provided the best agreement with the experimental data (R^2 = 0.9912 for linear fitting), indicating that CBB-G molecules were predominantly adsorbed as a monolayer on a finite number of energetically favourable adsorption sites distributed over the NiO@chitosan surface. The Temkin and Dubinin–Radushkevich models further suggested that the adsorption process was governed mainly by weak physicochemical interactions rather than irreversible chemical bonding (Foo and Hameed, 2010), which is also supported by the thermodynamic analysis indicating an endothermic adsorption process (ΔH° = 39.58 kJ mol^{-1}) (Hameed et al., 2008).

The proposed adsorption mechanism is further supported by the physicochemical characterization of the adsorbent. BET analysis revealed a mesoporous structure with a specific surface area of 34.56 m^2 g^{-1} and an average pore diameter of 12.29 nm, providing abundant accessible adsorption sites and facilitating diffusion of dye molecules into the bead structure. FE-SEM images shown in Figure 4 demonstrated that the bead surface became smoother after adsorption due to the deposition of CBB-G molecules, while the appearance of sulfur in the EDS spectrum confirmed successful adsorption of the dye (Tan et al., 2008). FTIR spectra (Figure 3b) showed shifts in the characteristic Ni–O, hydroxyl and amino group vibrations after adsorption, indicating the participation of these functional groups during the adsorption process (Sakkayawong et al., 2005). Furthermore, the pHpzc value of 7.75 suggests that electrostatic interactions contribute significantly to dye uptake near neutral pH, although the appreciable adsorption observed under the optimized conditions also indicates the contribution of hydrogen bonding and other weak intermolecular interactions (Ayawei et al., 2017; Tran et al., 2017). Collectively, these experimental observations suggest that CBB-G adsorption proceeds through a combination of external mass transfer, intraparticle diffusion, and adsorption at energetically favourable active sites within the NiO@chitosan composite (Ayawei et al., 2017; Plazinski et al., 2009). The molecular-level interactions responsible for this adsorption behaviour are further investigated using molecular docking simulations in the following section.

3.5 Proposed mechanism using molecular modeling and docking

The adsorption behaviour of CBB-G on the NiO@chitosan composite beads was investigated using molecular docking simulations. The computational analysis yields atomistic-level knowledge of molecular orientation, binding affinities and dominant intermolecular interactions of the composition that dictate the dyes' immobilization on the composite surface (Salahshoori et al., 2024). As shown in Figure 1a optimization molecular models of individual components further illustrate architectural and chemical characteristics of adsorption. This NiO model shows a cubic crystalline lattice comprised of periodically arranged Ni^{2+} and O^{2-} ions that is like the thermodynamically stable phase of nickel oxide by its structure. Chitosan polymer chain includes large number of hydroxyl (–OH) and amino ($–NH_2$)-functional groups distributed along the backbone which give multiple polar and protonatable active sites. CBB-G dye molecule is an extended π-conjugated aromatic framework with negatively charged sulfonate ($–SO_3^-$) functional groups and heteroatom-rich moieties. There is an excellent spatial complementarity between the electron-rich dye functionalities and positively charged domains of the composite on which interfacial interaction occurs. The adsorption mechanism on the composite surface is depicted in Figure 1b and docking was carried out without bounding the interaction to a given crystallographic plane. The NiO@chitosan composite exhibits a heterogeneous 3D structure that the NiO nanoparticles have embedded in the polymeric matrix providing accessible porous and hollow domain acting as the energetically favorable adsorption sites. When a minimum-energy docked configuration and Monte Carlo simulated annealing search have been performed, the CBB-G molecule undergoes spontaneous reorientation and sticks to an annealing site in the porous cavities rather than remaining shallowly adhered to the exterior surface (Fichthorn and Weinberg, 1991). This limited space within hollow areas suggest structural porosity and entry to the interior of the material promoting adsorption. The porous shape improves adsorption of dye by providing more effective surface area, facilitating spatial confinement effect, and creating large intermolecular contact between the adsorbate and the composite layer. The docked arrangement exhibit large interfacial affinity, when the aromatic backbone of CBB-G is aligned to facilitate the maximum surface contact, corroborating the influence of the porous design on the adsorption efficiency. Surface-specific interactions are explained further with adsorption from the crystallographic NiO (111) plane in Figure 1c. In the best adsorption design derived from docking simulations, the CBB-G molecule takes up an advantageous orientation with close interfacial contact with the exposed Ni^{2+} nuclei of the (111) surface and the functional groups of the chitosan matrix, and thus it shows preferential binding at energetically favorable sites. The optimal docked sequence reveals that the dye molecules are tightly bound to the NiO@chitosan surface, indicating a high interfacial affinity and highly accessible structurally active sites (Manokaran et al., 2025). The adsorption process is controlled by co-action of non-covalent interactions, which will be dominated by the electrostatic attraction providing the dominant stabilizing forces. More precisely, negatively charged sulfonate ($–SO_3^-$) groups and heteroatom-rich moieties within CBB-G effectively interact with positively charged protonated amino groups ($–NH_3^+$) of chitosan and positively polarized Ni^{2+} sites visible on the NiO (111) surface. The charge-driven interactions are critical for stabilizing the dye molecule when adsorbed at the adsorbent interface and consequently reducing docking interaction energy

10.3389/fceng.2026.1887485

TABLE 1 Inventory data for the material used production of beads and 1 m^3 treated water.

Stages	Input	Value	Units
Nickel oxide (NiO) nanoparticles production	Nickel chloride hexahydrate	17.6667	kg
	Ammonium hydroxide	14.8171	L
	Distilled water	142.022	L
Chitosan- NiO beads	NiO nanoparticles	5.56667	kg
	Chitosan	1.38889	kg
	Acetic acid	145.972	L
	Sodium hydroxide (NaOH)	6.94444	kg
	Distilled water	347.222	L
Wastewater treatment process	Chitosan-NiO beads	6.944444444	kg
	CBBG dye	0.013888889	kg
	Distilled water	2777.778	L
Stages	**Output**	**Value**	**Units**
Nickel Oxide (NiO) nanoparticles production	NiO nanoparticles	5.56667	kg
	NH_4Cl solution	150.7	L
	Water vapour	18.2502	L
Chitosan- NiO beads	Chitosan-NiO beads	6.94444	kg
	Water vapour	24.333	L
	Wastewater	475.806	L
Wastewater treatment process	Dye loaded NiO@chitosan beads	6.958333333	kg
	(dye-containing wastewater)	1777.777,778	L
	Column effluent	1,000	L

significantly. As well as electrostatic forces, hydrogen bonding interactions are formed between the hydrogen donors of the dye mainly–NH and–CH groups and the electronegative oxygen and nitrogen atoms on NiO@chitosan surface. Such directional interactions also reinforce dye immobilization and strengthen interfacial stabilization. Furthermore, van der Waals and π-surface dispersion interactions interact to stabilize adsorption due to the close proximity of the extended aromatic π-electron system of CBB-G and the polymeric backbone of chitosan to the surface atoms of the NiO molecules. These dispersion forces, although weak in isolation, allow for favourable molecular alignments and even surface packing of larger surface particles and thus strengthen the dye adsorbent systems in general as a whole (Tran et al., 2017). The molecular docking results were presented in Figure 1c confirm that the adsorption of CBB-G on the surface of NiO (111) occurs through synergistic processes comprising of electrostatic attraction, hydrogen bonding and van der Waals interaction along with high surface–dye adhesion, which is found at the exposed Ni^{2+} active sites. The large proportion of non-covalent interactions shows that the adsorption process is more physical than irreversible chemisorption. The inclusion of crystalline NiO (111) active sites together with functionalized chitosan matrix gives complementary binding domains, which accounts the experimentally observed exceptional adsorption efficiency of the NiO@chitosan composite toward the CBB-G dye.

Supplementary Figure S5 presents the distribution and relative probability of the adsorption energies for the CBB-G–NiO@chitosan system. A sharp and dominant peak centred at approximately −16 kcal mol^{-1} indicates that most adsorption configurations converge to a moderately negative energy state, suggesting that this is the most probable and energetically favourable adsorption configuration (Manokaran et al., 2025). The predominance of this energy region suggests that adsorption is mainly associated with weak to moderate non-covalent interactions rather than irreversible covalent bonding. In contrast, the less frequent peaks observed between −68 and −30 kcal mol^{-1} may correspond to localized interactions at specific active sites, such as exposed Ni^{2+} centres or protonated amino groups; however, their low probability suggests that these interactions do not dominate the overall adsorption process. Therefore, the adsorption energy distribution suggests that CBB-G adsorption onto the NiO@chitosan composite is predominantly associated with weak to moderate non-covalent interactions. When considered together with the optimized docking configurations, these results suggest that the adsorption process is likely to be governed mainly by reversible physisorption (Plazinski et al., 2009). This interpretation is consistent with the experimentally proposed adsorption mechanism, in which CBB-G molecules may initially diffuse through the porous structure,

TABLE 2 Inventory data for the energy used for 1 m^3 of treated water.

Name of the process	Type of instrument	Quantity	Unit
Nickel Oxide (NiO) nanoparticles production	Muffle furnace	14	kWh
	Magnetic stirrer	1.32	kWh
	Hot air oven	18	kWh
	Distilled water unit	35	kWh
	Vacuum filtration	0.38	kWh
Chitosan- NiO beads	Magnetic stirrer	1.32	kWh
	Distilled water unit	35	kWh
Wastewater treatment process	Peristaltic pump	32.63889	kWh
	Distilled water unit	35	kWh

TABLE 3 Environmental impacts for the two LCA studies with functional units being 1 kg of bead production and 1 m^3 of treated water.

Impact category	Unit	1 kg of bead production	1 m^3 of treated water
Climate change (GWP)	kg CO2-Eq	105.8052	852.6744803
Acidification: terrestrial	kg SO2-Eq	0.461,907	3.581487504
Eutrophication: freshwater	kg P-Eq	0.040994	0.385168362
Water use	m3	3.72512	26.23673413
Human toxicity: carcinogenic	kg 1,4-DCB-Eq	16.78984	131.9344193
Human toxicity: non-carcinogenic	kg 1,4-DCB-Eq	215.9404	1674.897303

occupy energetically favourable adsorption sites as a predominantly monolayer, and subsequently become stabilized through electrostatic attraction, hydrogen bonding, and van der Waals interactions (Ayawei et al., 2017).

3.6 Reusability and ecotoxicology analysis

In this study, the reusability of NiO@chitosan beads was explored with the aim to evaluate their stability and economic feasibility for reuse in cyclical sorption processes. Beads were collected after each experiment and washed with distilled water to remove any remaining adsorbate followed by drying at room temperature. This was repeated in the sorption experiments to assess the quality of these same regenerated beads. As illustrated in Supplementary Figure S6 (see ESM), NiO@chitosan beads also have nearly homogenous removal efficacy up to the fourth cycle proving their potential for reuse as an independent sorbent system (Lau et al., 2023). A bit longer equilibrium time was identified (10–15 min more time), which were incorporated into the time of sorption during the second and fourth cycles re-sampling. This delay probably resulted from the surface partial saturation and small structure adjustments when the bead matrix was used. The high removal efficiency of NiO@chitosan beads which was observed over multiple cycles is proved capable of the economical and eco-friendly water treatment with a significant recovery cycle. Simple regeneration, by washing, and air drying, is another feature that render them possible at high scales. Optimization of the bead composition and regeneration protocols is paramount to optimize the equilibrium kinetics and make them commercially viable as a reusable sorbent material.

The antibacterial action and elimination action of CBB-G dye was evaluated through the agar well diffusion procedure with *E. coli* (*E. coli*) as the strain for the test. Aerobically cultivated bacterial cells were developed in nutrient medium at 37 ˚C for 20 h, diluted to <106 cells/mL and inoculated onto agar plates. Wells with CBB-G dye solution, treated water, and deionized water were prepared, and the zones of inhibition were determined after overnight incubation. Reproducibility was validated through triplicate of all experiments. The presence of a 2.6 cm inhibition zone in the wells with water containing CBB-G was observed (Supplementary Figure S7) demonstrating the dye's ability to be antibacterial against *E. coli*. Conversely, wells in treated water and deionized control wells showed 100% growth of bacteria, with no remaining toxicity. These findings highlight that untreated CBB-G dye posed a threat to microbial communities, and CBB-G dye with processing water indicated its microbiological safety. NiO, in aqueous solutions, serves as an adsorbent to break down CBB-G dye. With no zones of inhibition found in treated samples it was expected that treatment with NiO strips the dye's antibacterial activity, meaning it has no adverse effect on non-target microorganisms. This is especially applicable to environmental usage as there seems to be a high potential of being discharged or reused with minimal eco-impact

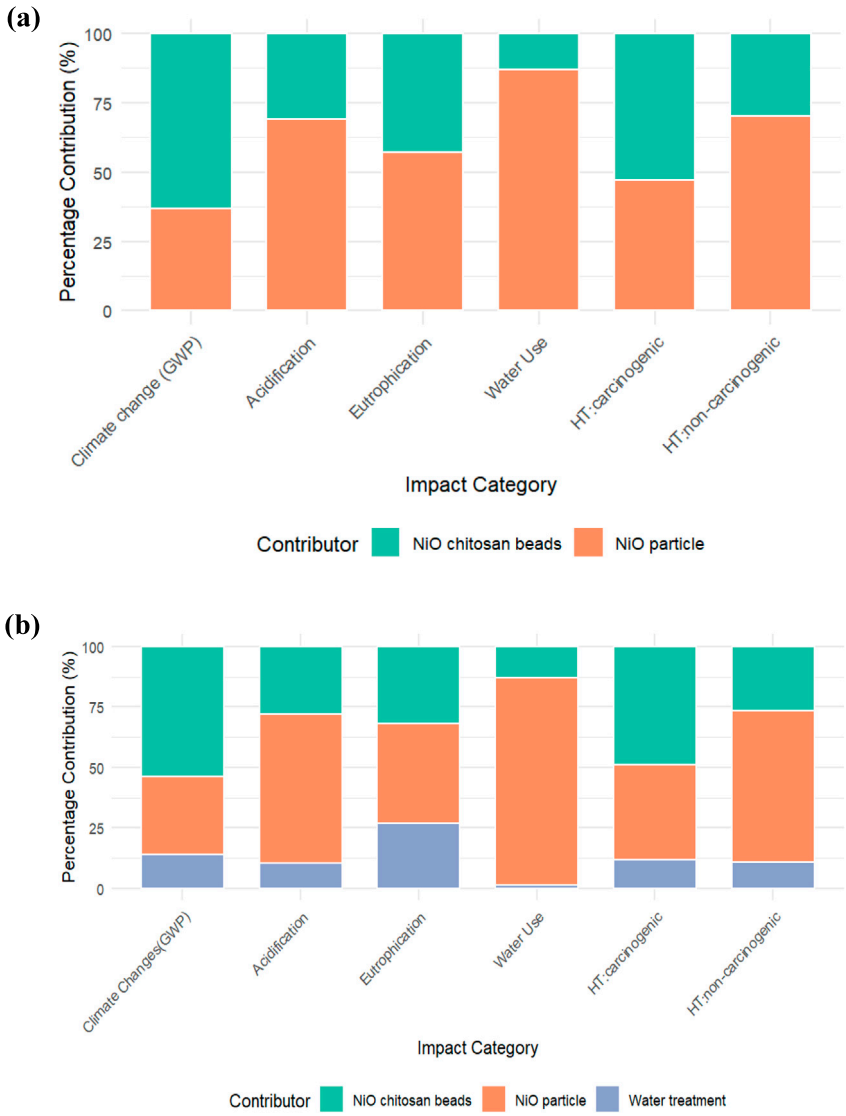

FIGURE 9
(a) Environmental impact of percentage contribution across different stages of the process of bead formation for impact categories like climate change (GWP), acidification, eutrophication, water use, human toxicity: carcinogenic, and human toxicity: non-carcinogenic; **(b)** Environmental impact of percentage contribution across different stages of the water treatment process for impact categories like climate change (GWP), acidification, eutrophication, water use, human toxicity: carcinogenic, and human toxicity: non carcinogenic.

in NiO-treated water. The results corroborate the previous literature on the effectiveness of NiO in dye adsorption and strengthen its potential as an environmentally sustainable remediation material (Zhao J. et al., 2021).

3.7 Gate-to-use life cycle assessment

The materials required for the synthesis of NiO@chitosan beads were lab grade reagents like $NiCl_2.6H_2O$, NH_4OH, and chitosan. The functional units during these studies were the production of 1 kg of beads and 1 m^3 of treated water from dye-contaminated water. Based on experimental investigation and process scale-up calculations, it was found that 6.94 Kg of such beads are required for the generation of 1 m^3 clean effluent from dye-laden wastewater. To the best of the authors' knowledge, no studies have been conducted to assess the environmental impact of NiO@chitosan beads for the dye-contaminated water sample treatment. Most of the inventory data considered during the production of beads and wastewater treatment are primary. However, some assumptions were made in the study, like, 1) A proxy process was used for the background processing of $NiCl_2.6H_2O$, 2) Chitosan production was not considered, as it was a lab-grade purchased reagent and its processing was out of the scope of this study, 3) Electricity consumption was modeled using the Indian electricity mix–Eastern Grid from ecoinvent, which accurately reflects the regional energy profile relevant to the study location. Tables 1, 2 have detailed inventory data on the production process of (6.94 kg) beads, along with wastewater treatment and electricity used, respectively. These inventories form the basis for subsequent impact assessment and interpretation phases of the study. The present analysis was conducted for two different system boundaries, one

from gate to gate analysis and another from gate to use. The results from this analysis are presented in Table 3.

The first analysis was done from gate-to-gate for 1 kg of bead production. It was observed that the total GWP from the production of beads was about 105 kg CO_2 eq/kg, which is less compared to the production of other chitosan composite beads mentioned by Iqbal et al (2025). According to that study, the average GWP of porous chitosan beads produced is 0.91 kg CO_2 eq/g [910 kg CO_2 eq/kg], which is higher than the emissions from NiO@chitosan beads in the present study.

Electricity used was a common environmental hotspot in both studies. Apart from this, the main hotspot to GWP is from acetic acid production, which contributes 56.146 kg CO_2 eq/kg NiO@ chitosan beads produced. Another study by (Bisaria et al., 2024) stated that the GWP emissions for chitosan–modified Ni–Fe layered double hydroxide powder is between 61–90 kg CO_2 eq/kg of material, which is very close to the emissions of chitosan-NiO bead production in this study. This study had lower human toxicity when compared to the NiO@chitosan beads for both carcinogenic and non-carcinogenic emissions. The significant environmental footprints observed in non-carcinogenic toxicity, acidification, eutrophication, and water use are primarily attributed to the proxy data used for $NiCl_2.6H_2O$. This emphasizes the critical need for primary chemical processing data to ensure a more precise impact assessment.

To get a comprehensive view on particles' environmental performance in context to their dye removal capacity, an LCA was conducted from gate to use, with the functional unit being 1 m^3 of treated water. It was found that 2.7778 m^3 of dye-laden wastewater can be processed through the fixed-bed adsorption column employing 6.94 Kg synthesized beads, resulting in the production of 1 m^3 of treated water with the treated effluent meeting the WHO recommended discharge limits for clean water discharge. The LCA revealed total emissions of 853.206 kg CO_2 eq/ m^3 (or 0.853 kg CO_2 eq/kg) treated water, with acetic acid processing and electricity use identified as the primary hotspots. Apart from this, NH_4OH production and the proxy process for nickel chloride hex $NiCl_2.6H_2O$ ahydrate contributed significantly to GWP emissions. The environmental impact assessment of NiO@ chitosan beads production and its application in water treatment in multiple impact categories is summarized in Figure 9. Figure 9a shows the percent impact of individual steps in bead formation on critical environmental markers, such as climate change (GWP), acidification, eutrophication, water use, and human toxicity (both carcinogenic and non-carcinogenic). Figure 9b displays the impact distribution with respect to different phases of the water treatment operations and indicates the relative contribution of each stage to the overall environmental burden. These results provide a comprehensive understanding of the sustainability profile of both material synthesis and its practical application.

Gonzalez et al. (2022) investigated cadmium removal using silicate–titanite nanotube/chitosan (STNTs-Ch) beads (Gonzalez et al., 2022). The study revealed that production of beads had an impact of 2.3130 kg CO2-eq/g, i. e 2313.0 kg CO2-eq/kg of bead production, which is substantially higher than the 105 kg CO_2-eq/kg reported in the present study. In both studies, electricity consumption was identified as the dominant emissions hotspot, tied to nanomaterial/precursor synthesis (STNTs and NiO, respectively). The relative share of the use phase also differed: it accounted for only ~2% of total emissions in the recycled STNTs-Ch scenario, versus ~14% in the present study, indicating scope for further optimization of our wastewater treatment step by decreasing the amount of beads used and increasing the amount of efficiency. Furthermore, Gonzalez et al. (2022) reported that the STNTs-Ch beads maintained 100% removal efficiency after four reuse cycles, whereas the NiO@chitosan beads retained 36% removal efficiency after four cycles. These comparisons highlight that per-mass production and per-volume treatment performance can point in different directions, and both metrics are useful in contextualizing environmental performance across differing materials.

4 Conclusion

NiO@chitosan beads prepared by the co-precipitation technique showed great promise as an efficient and mechanically sound adsorbent for dye removal. Operating parameters played a critical role in the adsorption process, where the best adsorption performance was observed at 150 r/min agitation speed, 54 g/L adsorbent dosage, 30 mg/L dye concentration, neutral pH, and 30 °C, resulting in an improved removal of CBB-G dye. The pseudo-second-order kinetic model (R^2 = 0.9993) best characterized the adsorption behavior as strong adsorption between adsorbent and adsorbate; whereas the Langmuir isotherm ($R^2 \approx 0.9900$) implied monolayer adsorption on a homogeneous surface. In addition, the fixed-bed column studies were consistent with the model by Thomas and Yoon–Nelson, showing the feasibility of breakthrough characteristics prediction and the practicality for continuous systems. A lifecycle assessment from an environmental perspective showed substantial environmental impact of 852 kg CO_2-eq per m^3 of treated water, driven primarily by energy-intensive processes and chemical application. The 6.94 kg of beads per m^3 need indicates further optimization may be required. Renewable power and production alternatives for new plants is essential change to alleviate environmental burdens and increase the sustainability of large-scale water treatment systems.

Data availability statement

The original contributions presented in the study are included in the article/Supplementary Material, further inquiries can be directed to the corresponding authors.

Author contributions

SM: Conceptualization, Data curation, Formal Analysis, Investigation, Methodology, Validation, Visualization, Writing – original draft, Writing – review and editing. DK: Conceptualization, Data curation, Formal Analysis, Investigation, Methodology, Software, Validation, Visualization, Writing – original draft, Writing – review and editing. RK: Conceptualization, Data curation, Methodology, Project administration, Supervision, Validation, Writing – original draft, Writing – review and editing. SB: Writing – original draft, Writing – review and editing. B-HJ: Writing – original draft, Writing – review and editing. JN:

Conceptualization, Data curation, Formal Analysis, Funding acquisition, Investigation, Project administration, Resources, Software, Supervision, Validation, Visualization, Writing – original draft, Writing – review and editing. SC: Conceptualization, Data curation, Formal Analysis, Funding acquisition, Investigation, Methodology, Project administration, Resources, Software, Supervision, Validation, Visualization, Writing – original draft, Writing – review and editing. ST: Conceptualization, Data curation, Formal Analysis, Funding acquisition, Investigation, Methodology, Project administration, Resources, Software, Supervision, Validation, Visualization, Writing – original draft, Writing – review and editing.

Funding

The author(s) declared that financial support was received for this work and/or its publication. This work is supported by the DST_FIST Fund (SR/FST/ET-1/2023/1189). The study was funded by Mahindra University Internal Research Grant No. IRP/2024/8 and MU-VT ICRCT2 research grant No. MU-VT IARCT^2/TA-SCC/2025/07. This work was also supported by the National Research Foundation of Korea (NRF) grant funded by the Korean Government (MSIT) (RS-2025–00520940).

Acknowledgements

The authors thank the Honorable Founder, Chancellor, Vice Chancellor, and Management of KIIT Deemed to be University and Mahindra University for the required laboratory and other infrastructure facilities, visionary leadership, and Internal research grants of KIIT Deemed to be University and Mahindra University.

Conflict of interest

The author(s) declared that this work was conducted in the absence of any commercial or financial relationships that could be construed as a potential conflict of interest.

Generative AI statement

The author(s) declared that generative AI was not used in the creation of this manuscript.

Any alternative text (alt text) provided alongside figures in this article has been generated by Frontiers with the support of artificial intelligence and reasonable efforts have been made to ensure accuracy, including review by the authors wherever possible. If you identify any issues, please contact us.

Publisher's note

All claims expressed in this article are solely those of the authors and do not necessarily represent those of their affiliated organizations, or those of the publisher, the editors and the reviewers. Any product that may be evaluated in this article, or claim that may be made by its manufacturer, is not guaranteed or endorsed by the publisher.

Supplementary material

The Supplementary Material for this article can be found online at: https://www.frontiersin.org/articles/10.3389/fceng.2026.1887485/full#supplementary-material

References

Ahmad, A. A., and Hameed, B. H. (2010). Fixed-bed adsorption of reactive azo dye onto granular activated carbon prepared from waste. *J. Hazard. Mater.* 175 (1–3), 298–303. doi: 10.1016/j.jhazmat.2009.10.003

Aksu, Z., and Gönen, F. (2004). Biosorption of phenol by immobilized activated sludge in a continuous packed bed: prediction of breakthrough curves. *Process Biochem.* 39 (5), 599–613. doi: 10.1016/S0032-9592(03)00132-8

Alhumaimess, M. S., Alsohaimi, I. H., Alruwaili, K. A., El-Sayed, M. Y., Zhang, F., and Hassan, H. M. A. (2025). Efficient removal of methylene blue from water using a novel chitosan@trimesic acid adsorbent grafted with Dimercapto-1,3,4-Thiadiazole. *J. Polym. Environ.* 33 (12), 5236–5255. doi: 10.1007/s10924-025-03712-3

Arulkumar, M., Sathishkumar, P., and Palvannan, T. (2011). Optimization of Orange G dye adsorption by activated carbon of *Thespesia populnea* pods using response surface methodology. *J. Hazard. Mater.* 186 (1), 827–834. doi: 10.1016/j.jhazmat.2010.11.067

Ayawei, N., Ebelegi, A. N., and Wankasi, D. (2017). Modelling and interpretation of adsorption isotherms. *J. Chem.* 2017, 1–11. doi: 10.1155/2017/3039817

Bakhta, S., Sadaoui, Z., Bouazizi, N., Samir, B., Cosme, J., Allalou, O., et al. (2024). Successful removal of fluoride from aqueous environment using Al(OH)3@AC: column studies and breakthrough curve modeling. *RSC Adv.* 14 (1), 1–14. doi: 10.1039/d3ra06697e

Bisaria, K., Seth, C. S., and Singh, R. (2024). Life cycle assessment of chitosan modified Ni–Fe layered double hydroxide for arsenic(iii) sequestration in aqueous medium: comparison of the impacts of adsorbent recycling, instrument use and source of energy. *Environ. Sci. Adv.* 3 (8), 1153–1162. doi: 10.1039/D3VA00312D

Boricha, A. G., and Murthy, Z. V. P. (2010). Preparation of N,O-Carboxymethyl chitosan/cellulose acetate blend nanofiltration membrane and testing its performance in treating industrial wastewater. *Chem. Eng. J.* 157 (2–3), 393–400. doi: 10.1016/j.cej.2009.11.025

Crini, G. (2006). Non-conventional low-cost adsorbents for dye removal: a review. *Bioresour. Technol.* 97 (9), 1061–1085. doi: 10.1016/j.biortech.2005.05.001

de Sales, P. F., Magriotis, Z. M., Rossi, M. A. L. S., Resende, R. F., and Nunes, C. A. (2013). Optimization by response surface methodology of the adsorption of coomassie blue dye on natural and acid-treated clays. *J. Environ. Manag.* 130, 417–428. doi: 10.1016/j.jenvman.2013.08.067

Dhananasekaran, S., Palanivel, R., and Pappu, S. (2016). Adsorption of methylene blue, bromophenol blue, and coomassie brilliant blue by α-chitin nanoparticles. *J. Adv. Res.* 7 (1), 113–124. doi: 10.1016/j.jare.2015.03.003

El-Dossoki, F. I., Hamza, O. K., and Gomaa, E. A. (2024). *Thermodynamic, Kinetics, and Adsorption Mechanism Studies of Methyl Orange by Surfactant-Modified Activated Carbon*, 364–382. doi: 10.1007/978-3-031-62672-2_21

Fichthorn, K. A., and Weinberg, W. H. (1991). Theoretical foundations of dynamical monte carlo simulations. *J. Chem. Phys.* 95 (2), 1090–1096. doi: 10.1063/1.461138

Foo, K. Y., and Hameed, B. H. (2010). Insights into the modeling of adsorption isotherm systems. *Chem. Eng. J.* 156 (1), 2–10. doi: 10.1016/j.cej.2009.09.013

Forgacs, E., Cserháti, T., and Oros, G. (2004). Removal of synthetic dyes from wastewaters: a review. *Environ. Int.* 30 (7), 953–971. doi: 10.1016/j.envint.2004.02.001

Gonzalez, M. N. G., Quiroga-Flores, R., and Börjesson, P. (2022). Life cycle assessment of a nanomaterial-based adsorbent developed on lab scale for cadmium removal: comparison of the impacts of production, use and recycling. *Clean. Environ. Syst.* 4, 100071. doi: 10.1016/j.cesys.2022.100071

Gupta, V. K., and Suhas, (2009). Application of low-cost adsorbents for dye removal – a review. *J. Environ. Manag.* 90 (8), 2313–2342. doi: 10.1016/j.jenvman.2008.11.017

Hameed, B. H., Mahmoud, D. K., and Ahmad, A. L. (2008). Equilibrium modeling and kinetic studies on the adsorption of basic dye by a low-cost adsorbent: Coconut (*Cocos nucifera*) bunch waste. *J. Hazard. Mater.* 158 (1), 65–72. doi: 10.1016/j.jhazmat.2008.01.034

Hasmath Farzana, M., and Meenakshi, S. (2015). Photocatalytic aptitude of titanium dioxide impregnated chitosan beads for the reduction of Cr(VI). *Int. J. Biol. Macromol.* 72, 1265–1271. doi: 10.1016/j.ijbiomac.2014.09.029

Ho, Y.-S. (2006). Second-order kinetic model for the sorption of cadmium onto tree fern: a comparison of linear and non-linear methods. *Water Res.* 40 (1), 119–125. doi: 10.1016/j.watres.2005.10.040

Ho, Y. S., and McKay, G. (1998). A comparison of chemisorption kinetic models applied to pollutant removal on various sorbents. *Process Saf. Environ. Prot.* 76 (4), 332–340. doi: 10.1205/095758298529696

Ho, Y. S., and McKay, G. (1999). Pseudo-second order model for sorption processes. *Process Biochem.* 34 (5), 451–465. doi: 10.1016/S0032-9592(98)00112-5

Iqbal, F., Upadhyay, A., Tehrani, R., and Rowles, L. S. (2025). Evaluating environmental and economic sustainability of engineered chitosan particles for water treatment. *Clean. Mater.* 16, 100319. doi: 10.1016/j.clema.2025.100319

Jiang, R., Zhu, H.-Y., Zang, X., Fu, Y.-Q., Jiang, S.-T., Li, J.-B., et al. (2024). A review on chitosan/metal oxide nanocomposites for applications in environmental remediation. *Int. J. Biol. Macromol.* 254, 127887. doi: 10.1016/j.ijbiomac.2023.127887

Kannan, K., Radhika, D., Nikolova, M. P., Sadasivuni, K. K., Mahdizadeh, H., and Verma, U. (2020). Structural studies of bio-mediated NiO nanoparticles for photocatalytic and antibacterial activities. *Inorg. Chem. Commun.* 113, 107755. doi: 10.1016/j.inoche.2019.107755

Karakaya, Ş. N., Aylanç, A., Arar, Ö., and Arda, M. (2026). Removal of coomassie brilliant blue G-250 from aqueous solutions by anion-exchange resin. *Turkish J. Anal. Chem.* 8 (1), 42–50. doi: 10.51435/turkjac.1845865

Kjidaa, B., Mamouni, R., Aziz, K., Saffaj, T., Adraoui, I., Mchich, Z., et al. (2023). Green synthesis of a biomaterial composite based on fish scales for anionic dye removal: Characterization and optimization by RSM@BBD approach. *Water Air Soil Pollut.* 234, 352. doi: 10.1007/s11270-023-06341-5

Lai, K. C., Tee, W. T., Loh, N. Y. L., Hiew, B. Y. Z., Gan, S., and Lee, L. Y. (2024). Continuous adsorption of metanil yellow and remazol black B dyes onto fixed-bed of 3D graphene oxide/chitosan biopolymer. *South Afr. J. Chem. Eng.* 48, 276–284. doi: 10.1016/j.sajce.2024.02.007

Lau, K. S., Azmi, N. A. S., Chin, S. X., Zakaria, S., and Chia, C. H. (2023). Chitosan-bead-encapsulated polystyrene sulfonate for adsorption of methylene blue and regeneration studies: Batch and continuous approaches. *Polymers* 15 (5), 1269. doi: 10.3390/polym15051269

Mahmad Rozi, S. K., Saufi, N. A., and Mohammad Rashidi, N. A. N. (2023). Effective and fast adsorptive removal of coomassie brilliant blue G 250 dye from water using Fe_3O_4 magnetic nanoparticles. *Malays. J. Anal. Sci.* 27 (4), 849–864.

Manokaran, R., Aumond, T., Eck, J., Ergincan, O., Daniel, C., Farrusseng, D., et al. (2025). Molecular simulation of fluid adsorption in nanoporous adsorbents: simple descriptors for space decontamination applications. *Adsorption* 31 (5), 78. doi: 10.1007/s10450-025-00631-6

Morsy, M., Mostafa, K. M., Amyn, H. A.-M., El-Ebissy, A. A.-H., Salah, A. M., and Youssef, M. A. (2019). Synthesis and characterization of freeze dryer chitosan nanoparticles as multifunctional eco-friendly finish for fabricating easy care and antibacterial cotton textiles. *Egypt. J. Chem.* 62 (7), 1277–1293. doi: 10.21608/EJCHEM.2019.6995.1583

Noh, J. S., and Schwarz, J. A. (1989). Estimation of the point of zero charge of simple oxides by mass titration. *J. Colloid Interface Sci.* 130 (1), 157–164. doi: 10.1016/0021-9797(89)90086-6

Pham, T. M. H., Nguyen, N. S., Dao, T. N., Le, T. T., Nguyen, T. H., Pham, H. N., et al. (2022). Facile ultrasound-assisted green synthesis of NiO/Chitosan nanocomposite from mangosteen peel extracts as antibacterial agents. *J. Nanomater.* 2022, 2485291. doi: 10.1155/2022/2485291

Plazinski, W., Rudzinski, W., and Plazinska, A. (2009). Theoretical models of sorption kinetics including a surface reaction mechanism: a review. *Adv. Colloid Interface Sci.* 152 (1–2), 2–13. doi: 10.1016/j.cis.2009.07.009

Podoll, R. T., Irwin, K. C., and Brendlinger, S. (1987). Sorption of water-soluble oligomers on sediments. *Environ. Sci. and Technol.* 21 (6), 562–568. doi: 10.1021/es00160a006

Qi, L., Xu, Z., Jiang, X., Hu, C., and Zou, X. (2004). Preparation and antibacterial activity of chitosan nanoparticles. *Carbohydr. Res.* 339 (16), 2693–2700. doi: 10.1016/j.carres.2004.09.007

Rappé, A. K., Casewit, C. J., Colwell, K. S., Goddard, W. A., III, and Skiff, W. M. (1992). UFF, a full periodic table force field for molecular mechanics and molecular dynamics simulations. *J. Am. Chem. Soc.* 114 (25), 10024–10035. doi: 10.1021/ja00051a040

Rathika, G., Jagadeeswari, R., Sathiyapriya, T., and Selvakumar, P. (2024). Surface and quantum chemical parameters of nickel oxide nanostructures suited for ultraviolet-assisted cationic dye degradation. *Kuwait J. Sci.* 51 (2), 100200. doi: 10.1016/j.kjs.2024.100200

Raval, N. P., Shah, P. U., Ladha, D. G., Vekariya, M. K., Wadhwani, P. M., and Shah, N. K. (2017). Synthesis, characterization and adsorption significance of novel composite (chitosan beads loaded nickel-oxide nanoparticles). *Desalination Water Treat.* 62, 387–402. doi: 10.5004/dwt.2017.0308

Robinson, T., McMullan, G., Marchant, R., and Nigam, P. (2001). Remediation of dyes in textile effluent: a critical review on current treatment technologies with a proposed alternative. *Bioresour. Technol.* 77 (3), 247–255. doi: 10.1016/S0960-8524(00)00080-8

Sakkayawong, N., Thiravetyan, P., and Nakbanpote, W. (2005). Adsorption mechanism of synthetic reactive dye wastewater by chitosan. *J. Colloid Interface Sci.* 286 (1), 36–42. doi: 10.1016/j.jcis.2005.01.02

Salahshoori, I., Wang, Q., Nobre, M. A. L., Mohammadi, A. H., Dawi, E. A., and Khonakdar, H. A. (2024). Molecular simulation-based insights into dye pollutant adsorption: a perspective review. *Adv. Colloid Interface Sci.* 333, 103281. doi: 10.1016/j.cis.2024.103281

Salleh, M. A. M., Mahmoud, D. K., Karim, W. A. W. A., and Idris, A. (2011). Cationic and anionic dye adsorption by agricultural solid wastes: a comprehensive review. *Desalination* 280 (1–3), 1–13. doi: 10.1016/j.desal.2011.07.019

Shang, Y., Zhang, J., Wang, X., Zhang, R., Xiao, W., Zhang, S., et al. (2016). Use of polyethyleneimine-modified wheat straw for adsorption of Congo red from solution in batch mode. *Desalination Water Treat.* 57 (19), 8872–8883. doi: 10.1080/19443994.2015.1027280

Shi, Y., Wang, X., Feng, C., Chen, W., and Yang, S. (2024). Adsorption properties of natural zeolite supported by chitosan on Cd(II) in micropolluted irrigation water. *ACS Omega* 9 (1), 573–584. doi: 10.1021/acsomega.3c06041

Tan, I. A. W., Ahmad, A. L., and Hameed, B. H. (2008). Adsorption of basic dye on high-surface-area activated carbon prepared from coconut husk: equilibrium, kinetic and thermodynamic studies. *J. Hazard. Mater.* 154 (1–3), 337–346. doi: 10.1016/j.jhazmat.2007.10.03

Tran, H. N., You, S.-J., and Chao, H.-P. (2017). Fast and efficient adsorption of methylene green 5 on activated carbon prepared from new chemical activation method. *J. Environ. Manag.* 188, 322–336. doi: 10.1016/j.jenvman.2016.12.003

Vakili, M., Rafatullah, M., Salamatinia, B., Abdullah, A. Z., Ibrahim, M. H., Tan, K. B., et al. (2014). Application of chitosan and its derivatives as adsorbents for dye removal from water and wastewater: a review. *Carbohydr. Polym.* 113, 115–130. doi: 10.1016/j.carbpol.2014.07.007

Wang, S., and Peng, Y. (2010). Natural zeolites as effective adsorbents in water and wastewater treatment. *Chem. Eng. J.* 156 (1), 11–24. doi: 10.1016/j.cej.2009.10.029

Wang, H., Xing, H., Yan, K., Han, D., and Chen, J. (2022). Oyster shell derived hydroxyapatite microspheres as an effective adsorbent for remediation of coomassie brilliant blue. *Adv. Powder Technol.* 33 (2), 103425. doi: 10.1016/j.apt.2022.103425

Wang, K., Zhang, F., Xu, K., Che, Y., Qi, M., and Song, C. (2023). Modified magnetic chitosan materials for heavy metal adsorption: a review. *RSC Adv.* 13 (10), 6713–6736. doi: 10.1039/D2RA07112F

Weber, W. J., and Morris, J. C. (1963). Kinetics of adsorption on carbon from solution. *J. Sanit. Eng. Div.* 89 (2), 31–59. doi: 10.1061/JSEDAI.0000430

Yagub, M. T., Sen, T. K., Afroze, S., and Ang, H. M. (2014). Dye and its removal from aqueous solution by adsorption: a review. *Adv. Colloid Interface Sci.* 209, 172–184. doi: 10.1016/j.cis.2014.04.002

Yoon, Y. H., and Nelson, J. H. (1984). Application of gas adsorption kinetics I. A theoretical model for respirator cartridge service life. *Am. Industrial Hyg. Assoc. J.* 45 (8), 509–516. doi: 10.1080/15298668491400197

Zhang, X., Zhang, Z., Wu, W., Yang, J., and Yang, Q. (2021). Preparation and characterization of Chitosan/nano-ZnO composite film with antimicrobial activity. *Bioprocess Biosyst. Eng.* 44 (6), 1193–1199. doi: 10.1007/s00449-021-02521-x

Zhao, H., Wang, R., Deng, H., Zhang, L., Gao, L., Zhang, L., et al. (2021). Facile preparation of self-assembled chitosan-based POSS-CNTs-CS composite as highly efficient dye absorbent for wastewater treatment. *ACS Omega* 6 (1), 294–300. doi: 10.1021/acsomega.0c04565

Zhao, J., Wu, Q.-X., Cheng, X.-D., Su, T., Wang, X.-H., Zhang, W.-N., et al. (2021). Biodegradation and detoxification of the triphenylmethane dye coomassie brilliant blue by the extracellular enzymes from mycelia of lactarius deliciosus. *Front. Chem. Sci. Eng.* 15 (2), 421–436. doi: 10.1007/s11705-020-1952-7